_____

Unterschrift BetreuerIn

TU WIEN
TECHNISCHE
UNIVERSITÄT
WIEN
Vienna University of Technology

DIPLOMARBEIT

THE INFLUENCE OF CROSSLINKING ON THE THERMORESPONSIVE BEHAVIOUR OF POLYMER BRUSHES

ausgeführt am Institut für Angewandte Chemie

der Chalmers University of Technology, Göteborg

unter der Anleitung von

Associate Prof. Dr. Andreas B. Dahlin

(Chalmers University of Technology)

&

Assistant Prof. Miriam M. Unterlass

(TU Wien)

durch

Sophia Thiele

geboren am 26.07.1995

Matrikelnummer: 01426839

sophia_thiele@hotmail.com

April 23, 2020

Unterschrift StudentIn

Acknowledgements

Firstly, I wish to show my gratitude to Dr. Andreas Dahlin who enabled my work on this fascinating project in Gothenburg. I have learned a lot, scientifically and personally, throughout the last months. I would also like to pay my special regards to my colleague and friend Dr. Rebekah Hailes for her professional support throughout the whole research and writing process, our fruitful work-related and friendly discussions, great after-work evenings, and climbing sessions. Our developing friendship was truly one of the best parts of the last year. Moreover, thank you to my other colleagues from the research group. Thank you Gustav, John, Jolie, Marika, Oliver, and Justas for creating a good working atmosphere with great music, funny comments and in particular for your helpfulness. It was a pleasure to work in this group.

I would like to thank Anne Wendel for XPS measurements, and the Chalmers materials analysis laboratory (CMAL) for enabling the SPR experiments.

I wish to express my deepest gratitude to Prof. Miriam Unterlass for her co-supervision at TU Vienna, and most importantly for sharing her knowledge, giving valuable advice throughout my studies, and enabling a fantastic project for my BSc thesis together with Dr. Michael Taubländer. This has all contributed hugely to my professional and personal development.

It is important for me to thank my family and close friends who have supported me throughout my whole life. Many thanks to my parents Nicole, Johann, and Günther for enabling my studies with their financial support, for many encouraging and motivating discussions, and for their willingness to listen to my worries; Thank you for reminding me of priorities other than a successful career when necessary, and in particular for raising my interest and curiosity in so many things throughout a great childhood: mountaineering, foreign cultures, horse riding and science.

And at this point, thanks to the best partner, Tobi, for staying with me in difficult times, calming me down when necessary, and for all those unforgettable moments we have had together. Besides my family and Tobi, my closest friends were always there when I needed them, and I wish to thank Julia, Isa, Lena, Esi, Fe, Kathi, Jana, and the best study colleagues Carina, Eva, and Meru for so much fun, unforgettable moments and a great friendship. Thanks to Kathi and Fabian who shared a flat with me in Vienna – I will never forget the amazing time we have had together.

Kurzfassung

Poly(N-isopropyl acrylamide) (PNIPAM) gehört zur Kategorie der thermoresponsiven Polymere: bei Raumtemperatur wasserlöslich, bei Temperaturen ab 32 °C kollabierend in einem sogenannten "coil-to-globule" Übergang. Gebunden an Oberflächen in mikrofluidischen Kanälen werden poly(N-isopropyl acrylamide) (PNIPAM) Bürsten bereits als temperaturkontrollierte Ventile, Pumpen und Filter eingesetzt.[1,2,3] Dabei sind kontrollierbare, der Anwendung angepasste Eigenschaften sowie Stabilität gegen Hydrolyse besonders wichtig. Vernetzte Polymerbürsten zeigen höhere Stabilität gegen Hydrolyse,[4,5] außerdem ermöglichen Vernetzer eine kontrollierte Variation der Übergangstemperatur,[6] Durchlässigkeit,[7] und das Einschleusen von molekularer Ladung (z.B. Medikamente).[6] Eine besonders wichtige Kenngröße in mikrofluidischen Kanälen ist das Verhältnis der Polymerschichtdicke von geschwollenem zu kollabiertem Zustand, welches bestimmt ob der Kanal komplett mit Polymer bedeckt oder die Wände nur beschichtet sind. In dieser Arbeit wurde der Effekt von zwei, einem *in-situ* (methylene bisacrylamide (MBAM)) und einem *ex-situ* (N-benzophenyl N-acrylamide (NBPAM)) Vernetzer auf das thermoresponsive Verhalten von PNIPAM Bürsten auf Gold Oberflächen untersucht. Unter Verwendung von surface plasmon resonance (SPR) und quartz crystal microbalance with dissipation monitoring (QCM-D) konnte demonstriert werden, dass die thermoresponsiven Eigenschaften mit zunehmendem Vernetzeranteil geschwächt werden, bis hin zu ihrem kompletten Verschwinden. Dies wurde bereits bei nur 1 mol% NBPAM, jedoch erst bei 4 mol% MBAM Gehalt erreicht. Außerdem wurde gezeigt, dass Vernetzergehalt, Lösungsmittel, und Reaktionszeit die Schwelleigenschaften und Reaktionskinetik beeinflussen.

Inspiriert durch den nuclear pore complex (NPC) wurden die PNIPAM-co-MBAM Gele als Tore für potentiell kontrolliere Protein Translokation in Nanoporen auf Gold Oberflächen getestet. Tatsächlich konnten poly(N-isopropyl acrylamide)-*co*-methylene bisacrylamide (PNIPAM-co-MBAM) Gele mit 1 mol% Vernetzergehalt den Proteinfluss kontrollieren. Da Proteine oft Indikatoren für bestimmte Krankheiten sind, könnte dies ein erster Schritt in Richtung eines optischen Sensors für die Analyse von Krankheiten und spätere Entwicklung einer Therapie sein. Die tatsächliche Entwicklung eines solchen Sensors liegt jedoch weit außerhalb des Rahmens dieser Arbeit.

Abstract

Poly(N-isopropyl acrylamide) (PNIPAM) belongs to the category of thermoresponsive polymers: while water soluble at room temperature, it undergoes a coil-to-globule transition at 32 °C. Surface-attached PNIPAM brushes have served as thermo-controllable valves, pumps and filters inside microfluidic devices.[1,2,3] Controlled, adjusted properties and high stability agains hydrolysis are crucial if applied in microfluidic devices. Introducing crosslinks to polymer brushes allows for tuning of the lower critical solution temperature (LCST),[6] permeability,[7] and for incorporating molecular cargo (*e.g.* drugs).[6] An important parameter with respect to microfluidic channels is the polymeric layer thickness ratio in the swollen and collapsed state, as it determines if a channel diagonal is fully covered or only coated. This thesis investigates the effect of an *ex-situ* (*N*-benzophenyl *N*-acrylamide (NBPAM)), and *in-situ* (methylene bisacrylamide (MBAM)) crosslinker on the thermoresponsive behaviour of PNIPAM brushes grafted from gold surfaces. Using surface plasmon resonance (SPR) and quartz crystal microbalance with dissipation monitoring (QCM-D), we showed that increasing the percentage of crosslinker diminishes the thermoresponse of the network, up to a point where it vanishes completely. This point was reached at just 1 mol% for NBPAM, whereas PNIPAM-co-MBAM remained thermoresponsive up to 4 mol% crosslinker content. Furthermore, we demonstrated that crosslinker, solvent, and reaction time influence the swelling behaviour and reaction kinetics. Inspired by the NPC, the PNIPAM-co-MBAM gels were tested as gates towards protein translocation on nanopore patterned gold surfaces. Notably, we could demonstrate controlled protein gating for PNIPAM-co-MBAM with 1 mol% crosslinker content (Figure 0.1). As proteins often indicate diseases, trapping them in a controlled manner might later allow for the analysis of diseases and following treatment developments. However, the development of a related device is far beyond the scope of this work.
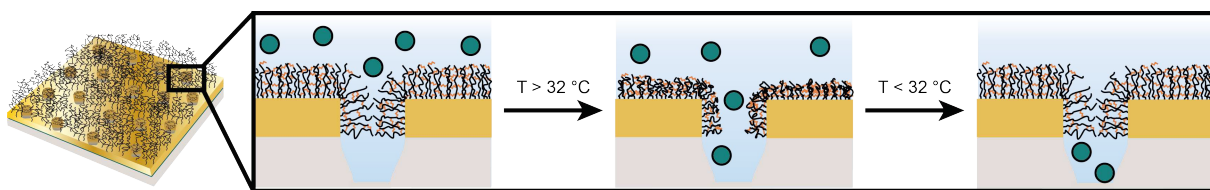
Figure 0.1.: PNIPAM-co-MBAM based gates inside nanowells on gold surfaces. At room temperature, the swollen gel forms an impenetrable barrier for proteins, whereas the gel allows for translocation upon collapsing above 32 °C.

Contents

Contents

List of Abbreviations and Symbols

AFM atomic force microscopy

AGET ATRP activators generated by electron transfer ATRP

ARGET-**ATRP** activators regenerated by electron transfer ATRP

ATRP atom-transfer radical polymerization

BSA bovine serum albumine

CRP controlled radical polymerization

D energy dissipation

DMF dimethylformamid

DMSO dimethylsulfoxide

DTBU Bis[2-(2-bromoisobutyryloxy)undecyl] disulfide

E$_{el}$ elastic energy

E$_{int}$ interaction energy

eq equivalent

FRP free radical polymerizations

f frequency

f$_R$ resonance frequency

FT-**IR** Fourrier transformation infrared spectroscopy

^{1}H-**NMR** proton nuclear magnetic resonance

h height

IEP isoelectric point

k_{act} activation rate constant

K_{ATRP} reaction constant for atom transfer radical polymerization

k_{deact} deactivation rate constant

Contents

k_p polymerization rate constant

k_t termination rate constant

LCST lower critical solution temperature

l_d penetration depth

LZ lysozyme

m mass

MBAM methylene bisacrylamide

M$_n$ number average molecular weight

mQ mili-pore water

M$_w$ mass average molecular weight

MFDs microfluidic devices

n refractive index

NIPAM N-isopropyl acrylamide

NBPAM N-benzophenyl N-acrylamide

NMP nitroxide-mediated polymerization

NPC nuclear pore complex

p pressure

PAA poly(acrylic acid

PAAM poly(acryl amide)

PBS phosphate buffered saline

PDEAAM poly(N,N-diethylacrylamide)

PE poly(ethylene)

PEG poly(ethylene glycol)

PEO poly(ethylene oxide)

PET poly(ethylene therephtalate)

PI isoelectric point

PMDEGA poly(monomethoxy diethyleneglycol acrylate)

PMDETA N,N,N',N'',N''-pentamethyldiethylenetriamine

PNIPAM poly(N-isopropyl acrylamide)

PNIPAM-co-MBAM poly(N-isopropyl acrylamide)-co-methylene bisacrylamide

PNIPAM-co-NBPAM poly(N-isopropyl acrylamide)-co-N-benzophenyl N-acrylamide

PVA poly(vinyl alcohol)

PVCL poly(N-vinylcaprolactam)

PVME poly(vinyl methyl ether)

QCM quartz crystal microbalance

QCM-D QCM with disspation monitoring

R_g radius of gyration

RAFT reversible addition fragmentation chain transfer

RBF round bottom flask

SAM self-assembled monolayer

SDS sodium dodecyl sulfate

SI-ATRP surface-initiated atom transfer radical polymerization

SI-ARGET-ATRP surface-initiated activators regenerated by electron transfer ATRP

SP surface plasmon

SPR surface plasmon resonance

T$_d$ decomposition T

T$_g$ glass transition T

T$_m$ melting T

Contents

TEM transmission electron microscopy

TIR total internal reflection

UCST upper critical solution temperature

VPTT volume phase transition temperature

**XPS** x-ray photoelectron spectroscopy

1. Introduction

Emerging technologies in the medical sector are flourishing. From efficient drugs, precisely controllable prosthesis[8] and 3D-printed organs[9], immense advances shape the current decade. Regardless, untreatable diseases are one of our greatest concerns. The first step for treating any new disease pertains its detection. At the onset, biomarkers that give rise to diseases (*e.g.* proteins) might be rare. Microfluidic devices (MFDs) provide an elegant way to handle small sample amounts. Analyte separation, collection and analysis can take place on one single chip which contains nm thin channels, reaction chambers and in- and outlets.[10,11] Controlled protein transport of the analyte to the detector in MFDs is of utmost importance to prevent false posiive results.[12] To achieve this, stimuli responsive polymers may serve as filters, valves or pumps.[1,2,3] These materials respond to small changes in their environment such as solvent composition,[13] pH,[14] and/or temperature[15]. Advances in radical polymerizations have enabled the synthesis of polymers grafted from surfaces involving a variety of chemical functionalities,[16,17,18] architectures,[19] and responsive behaviours. Responsive polymers can either block,[20] filter,[3] or reversibly trap and release proteins,[21,22] all potentially useful in the diagnosis of diseases. A detailed knowledge of how materials respond to an external stimuli is crucial for its application in MFDs. One example is a stimuli-controlled polymeric valve comprised of PNIPAM. A surface attached PNIPAM film swells in aqueous media at room temperature, whereas it collapses (*i.e.* reduces its thickness by expelling water) above $\approx 32\,°C$. Thus, PNIPAM brush valves in nanofluidic channels at femtoliter flow rates allowed or hindered solvent flow depending on the temperature.[23] The permeation properties of polymers alter upon introducing small structural changes such as crosslinks. Thus, crosslinked PNIPAM networks may have novel function inside MFDs, *e.g.* as a filter for proteins in the label-free detection of rare disease biomarkers. A detailed knowledge of the network's properties is crucial prior to its application. Therefore, the influence of crosslinking on the thermoresponsive behaviour of PNIPAM brushes was investigated in this work. Protein permeability of the same films inside gold coated solid-state 80-90 nm thin pores was also monitored. An overview of the theoretical background is given in the next section, followed by a discussion of the obtained results.

2. Theoretical Background

2.1. Surface Tethered Polymers and Networks

2.1.1. Polymer Brushes

Polymer chains bound to a supporting surface in close proximity to oneother (*i.e.* with high grafting density) are referred to as polymer brushes. "Close proximity" is defined in relation to the radius of gyration (R_g), which is given in Equation 2.1 where a is the Kuhn length and N the number of segments. In solution, three interactions must be considered for polymer brush chains: polymer-solvent, polymer-polymer and polymer-surface. For surface tethered polymers of lower grafting densities it is mostly the latter, interactions with the surface, that influences the chain conformation: on weakly attracting or repelling surfaces, "mushroom" conformations are observed (Figure 2.1**C**), whereas polymers attracted to the surface collapse (Figure 2.1**B**).[24]
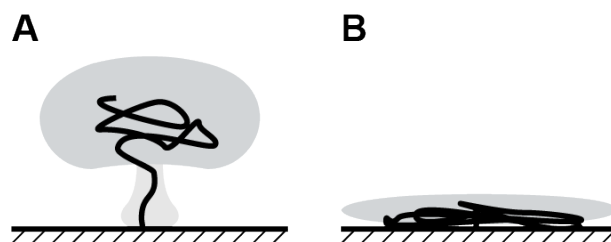
Figure 2.1.: Schematic of polymeric chains at low grafting density in solution. **A** A "mushroom" configuration occurs if the interactions with the surface are weakly attractive or repulsive, whereas in **B** the chains collapse if attracted by the surface.

For chains with a much smaller average distance between each other on the surface than the R_g (*i.e.* polymer brushes) the solvent quality determines their conformation.[25] Any solvent at certain pressure (p) and temperature is classified as poor, θ or good. At θ conditions, polymer-polymer and polymer-solvent interactions are perfectly balanced.[26,27] In good solvents, polymer brushes aim to reduce unfavourable polymer-polymer interactions, increase interactions with solvent, and thus elongate.[28] But, stretching limits the number of possible random-walk configurations for solvated brushes *i.e.* it decreases the entropy. The energetic equilibrium between these has two extremes: highly stretched brushes (minimal interaction energy), and highly entangled conformations (minimal elongation energy) as shown in Figure 2.2.[29] With decreasing solvent quality, polymer-polymer interactions are more energetically favoured and the equilibrium is shifted towards highly entangled brushes. This transition is referred to as coil-to-globule.[30]
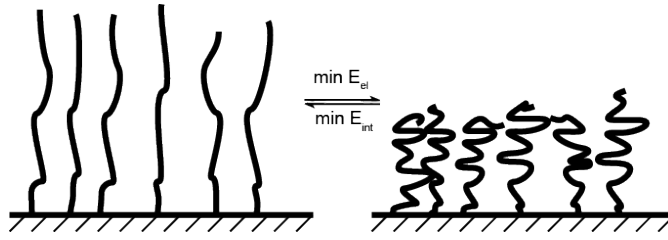
Figure 2.2.: Energetic equilibrium between the minimal interaction energy (E_{int}) and the minimal elastic energy (E_{el}) for a polymer brush in a good solvent.

ALEXANDER and DE GENNES modelled brushes in solvents. They consider the polymers as a uniform layer, all ending at the same distance L. In this case, Equation 2.2 holds for the brush concentration ϕ (in %), where N is the number of chain segments, a is the Kuhn length, and d is the distance between the anchoring points.[31,32] Hence, the height in the equilibrium state between E_{el} and E_{int} depends on the grafting density ($\sigma/\frac{chains}{nm^2}$) and the surrounding medium. Considering polymer brushes, Equation 2.3 holds for good solvents, whereas Equation 2.4 describes the height in poor solvents close to θ-conditions. Notably, in both cases the height scales directly with N – *i.e.* with the molecular weight.[29] This is important for kinetic studies of polymer brush synthesis strategies, where direct information can be extracted from their height.

$$R_g = N^{\frac{1}{2}} * a \tag{2.1}$$

$$\phi = \frac{N * a^3}{d^2 * L} \tag{2.2}$$

$$h \propto N * \sigma^{\frac{1}{3}} \tag{2.3}$$

$$h \propto N * \sigma^{\frac{1}{2}} \tag{2.4}$$

Polymer brushes can have different configurations, depending on the grafting density, molecular weight, and their inter- and intramolecular interactions between the surface, solvent, and brush. If polymer brushes switch between conformations in response to environmental changes such as solvent,[13] pH,[14] or temperature,[15] they are referred to as "smart" polymers. Responses from a smart brush could involve changes in solubility, shape, volume, conformation or physical state (*e.g.* a common phase transition).[33] This work focuses on thermoresponsive polymers, where a temperature change triggers a phase transition.
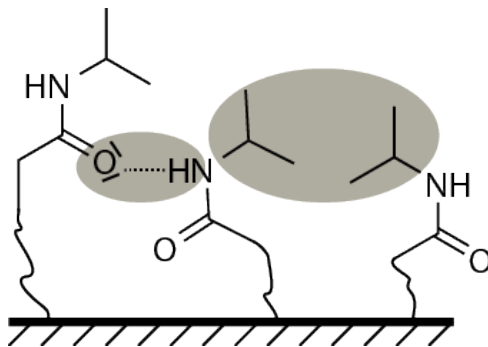
2.1.2. Thermoresponsive Polymers

In the literature, the term "thermoresponsive" for a polymer is clearly defined and distinguished from a common physical phase transition. Semi-crystalline polymers soften at the glass transition T (T_g), melt at melting T (T_m) and decompose at the decomposition T (T_d). Typically, the temperature gap between these transitions is huge. In contrast, the term "thermoresponsive" defines a material that experiences large property changes already upon *small* temperature variations (*e.g.* an increase from 10 °C to 25 °C).[13,15,34]

Thermoresponsive polymers are particularly interesting since temperature variations are applicable in many set-ups. For example, thermoresponsive materials served as biocompatible carriers in drug delivery systems,[35] as flow control valves in microfluidic chips,[36] and as temperature-controlled circuit breaker in electronic devices.[37] The temperature at which conformation transitions happen is differentiated into upper critical solution temperature (UCST) and LCST, depending on the phase diagram of the polymer in a certain solvent.[38] The polymer exhibits an UCST if it dissolves upon a temperature increase, a behaviour which is observed for poly(ethylene oxide) (PEO) and poly(vinyl alcohol) (PVA) in water.[39] If the solubility decreases above a certain temperature, and the polymer precipitates or films collapse, this is called the LCST. LCSTs in aqueous solutions are observed for poly(monomethoxy diethyleneglycol acrylate) (PMDEGA)[40], poly(N-vinylcaprolactam) (PVCL)[5], poly(ethylene glycol) (PEG),[41] PNIPAM and various copolymers containing them.[42,43]

PNIPAM has been extensively studied as a thermoresponsive polymer. It is highly promising for bio-related applications due to its LCST at 32 °C under physiological conditions (*i.e.* in aqueous media) and enhanced stability against hydrolysis compared to *e.g.* PVCL.[4,5] For PNIPAM in aqueous media, the hydrophilic amide moiety competes with the hydrophobic isopropyl group: H-bonding between water and the amide opposes inter- and intramolecular H-bonds between the polymeric chains[44] and hydrophobic interactions between the isopropyl groups. Simulations of the H-bonding in PNIPAM revealed that the –NH–group does not contribute significantly to the coordination of water molecules below the LCST, presumably due to steric hinderance from the isopropyl group. In contrast, the carbonyl oxygen readily H-bonds with polar solvents.[45] The interactions between PNIPAM chains are depicted in Figure 2.3. Since the number of possible chain conformations is higher in the collapsed state, the entropic gain is a major driving force for the sudden deswelling behavior of PNIPAM above its LCST.[46] Simultaneously, most of the water is expelled causing the characteristic chain-to-globule transition.[47] This thermoresponsive behaviour is typically retained in PNIPAM containing copolymers, though slightly altered.[46] Thus, the properties of polymer brushes can be tuned by introducing

new functional groups, steric hindrance, or crosslinks. Countless crosslinkers are available, varying in *e.g.* length, chemical nature, or crosslinking mechanism. Crosslinkers that introduce a completely new behaviour (*e.g.* electrolyte monomers) are beyond the scope of this work. Here the focus lies on the effect crosslinking itself has on the properties of PNIPAM brushes. Only crosslinkers with a similar chemical nature to PNIPAM were considered, and potential investigated effects reviewed briefly in the following section.

Figure 2.3.: Schematic of the intermolecular H-bonding between N–H and C=O and hydrophobic interactions between isopropyl groups.

2.1.3. Crosslinked Thermoresponsive Polymer Brushes

In solution, three dimensional connected networks that contain at least 10 % aqueous medium are defined as hydrogels. Strong covalent bonds (chemical hydrogels) or weaker interactions such as ionic and hydrogen bonds (physical hydrogels) make up these connections.[48] Physical crosslinks are usually reversible whereas chemical hydrogels are permanently crosslinked. The scope of hydrogels is broad: they are used as cultivation matrix for cells, stabilizers for particles, drug delivery systems, and (self-healing) coatings, amongst other applications.[49] Moreover, depending on their chemical nature, hydrogels can be bioinert (*e.g.* anti-fouling coatings for implants) or bioadhesive (*e.g.* cell-culture media, synthetic tissue or cartilage). In such applications, the gels are often attached to surfaces. Covalent bonds between a solid interface and the network cause confinement in one direction, and surface attached networks are reported to swell less compared to their nonattached counterparts.[50] Similarly, the swelling behaviour of polymer brush networks changes depending on the degree of crosslinking. For instance, crosslinked poly(acryl amide) (PAAM) brushes were observed to swell less compared to their uncrosslinked counterparts.[51] For "smart" surface attached networks, it was reported that they usually retain any responsive behavior after crosslinking.[44,52] Covalently crosslinked PNIPAM gels grafted on nanoparticles or smooth surfaces did indeed still display thermoresponsive behaviour.[46,53,54] However, chain-to-globule transitions must be clearly distinguished between for polymer brushes and networks (comparable to linear polymers in solution *vs.* hydrogels, respectively). PNIPAM networks at solid-liquid interfaces undergo a volume

transition (*i.e.* shrinkage) instead of a solubility change (*i.e.* precipitation) upon temperature increase. Hence, what is called LCST for polymer brushes is referred to as volume phase transition temperature (VPTT) for their crosslinked counterparts.[46]

In a good solvent, brushes of high grafting density typically show a stepwise decay in their concentration profile with increase distance from the surface,[55] in agreement with the ALEXANDER and DE GENNES model (see subsection 2.1.1). Models showed a similar concentration profile for surface-attached networks, although with a decrease in lubrication since few brush ends reach out into solution,[56] a behaviour that was later confirmed experimentally.[57] Crosslinking also diminishes degrafting of brushes in aqueous and organic solvents – *i.e.* increases their stability and improves the anti-fouling behaviour.[58,59] The strength of the crosslinks also plays a key role in the stability of brush networks: physical crosslinks in PNIPAM gels broke in dimethylsulfoxide (DMSO), whereas use of covalent crosslinker MBAM produced gels that were stable in DMSO, water, and aqueous sodium dodecyl sulfate (SDS) solutions.[60] Crosslinking also alters the mechanical properties, roughness, and swelling behaviour of polymer brushes. LILGE *et al.* prepared PAAM gels *via* surface-initiated atom transfer radical polymerization (SI-ATRP) from gold surfaces with varying crosslinker content (MBAM, 1 %-20 %). The covalently crosslinked PAAM networks showed reduced thicknesses in the swollen state with increased crosslinker content, despite similar dry heights.[61] This reduced swelling was also observed in models of crosslinked polymer brushes.[56] Confinement introduced by the crosslinks causes the reduced swelling behaviour. Moreover, the wettability was altered upon crosslinking.[62] Surface-attached networks showed overall lower water contact angles than brushes – *i.e.* higher wettability.

With regard to PNIPAM brushes, crosslinking is expected to alter the thermoresponsive behaviour in addition to the above-mentioned properties. Influenced thermoresponsive characteristics could be:

i) LCST

ii) permeability towards nanoparticles below and above the LCST

iii) swell- and collapse behaviour (*i.e.* brush height above and below the LCST)

By introducing 1 % or 2 % of a covalent crosslinker, the LCST of PNIPAM brushes on gold nanoparticles could be shifted from 32 °C to a VPTT of 34 °C.[6] In the same study, the authors observed different pore sizes for gels containing a varied amount of crosslinker. Transmission electron microscopy (TEM) images indicated that empty voids are retained in crosslinked brushes in air, whereas pure brushes form a more compact layer. It was observed in other studies that upon soaking thermoresponsive gels in aqueous solutions, voids are filled first before the layer thickness increases.[40,63,64] In contrast, PNIPAM

brushes swell immediately when exposed to water – *i.e.* there are no voids to be filled first.

In bulk PNIPAM-co-MBAM gels, the thermoresponsive behavior vanishes above $\approx 5\,\%$ MBAM crosslinker content.[65] However, high crosslinking was necessary for those gels to retain their shape.[34] A surface to which the crosslinked brushes are attached is expected to enhance their conformational stability. To destroy a surface-attached network, covalent bonds between the solid support and network (*e.g.* strong Au-S bonds[66] for gold surfaces) must be broken. Hence, examining the swell- and collapse behaviour of surface-tethered networks is particularly interesting for networks containing low amounts of crosslinkers.[53] While PNIPAM hydrogels have been exclusively prepared *ex-situ* and then attached to solid supports (mostly *via* spin-coating),[63,67] similar studies for PNIPAM networks grafted from flat solid surfaces are missing.

In another study by MA *et al.*, PNIPAM based networks grafted from surfaces were tested towards permeability of inorganic nanoparticles and biomacromolecules, but the influence on the swelling behaviour was not investigated.[7] Intuitively, the permeability highly depends on the pore shape and size inside the gel (*i.e.* available space between the polymer chains). Pore diameters increase with the size of the crosslinker used. For a bulk hydrogel with a macromolecular crosslinker, pore diameters up to 210 nm in the swollen state were prepared.[68] It was demonstrated that proteins could enter the gel in the swollen state, were trapped inside upon a temperature increase above the LCST, and left again by decreasing the temperature. This catch-and-release behaviour was retained for 3.5 nm gold particles in PNIPAM networks with 1 % of a smaller crosslinker (MBAM) attached to spherical silica nanoparticles.[6]

It is essential to possess information about the VPTT, permeability and swelling behaviour for future applications of PNIPAM-based brush networks. If the properties are well known, these gels could serve as thermo-controlled valves to hinder or enable translocation of particles in nano-sized channels. For biosensing applications in nanopores, the gels could act as so-called "gates" – a term that is described in detail in the following subsection.

2.2. Thermoresponsive Gates Inside Solid-State Nanopores

The term "gate" frequently appears in microbiology and cell studies.[69,70,71,72,73] There, a gate is typically connected to protein translocation through membranes, *e.g.* between cytoplasm and cell organelles such as mitochondria[72], chloroplasts[73] or the NPC[74]. The

latter has fascinated scientists for decades.[71,74,75] It enables a highly controlled translocation between cytoplasm and nucleus by filtering particles varying in chemical nature and size (*e.g.* ions, proteins and sugars) with different mechanisms at the same time: small particles translocate *via* diffusion through the NPC, whereas larger complexes are actively transported inside by attaching to shuttles which then diffuse through.[76] All of the details of its exact chemical composition, operation modes and accuracy are yet to be revealed. In mammals, it is a huge macromolecular complex of $\approx$125 MDa[76] that might never be fully resolved,[77] but artificial copies comprised mainly of polymers were prepared for a bottom-up study.[78] The structure of the NPC has inspired new approaches in microfluidic devices. Comprised of an outer ring functionalized with brush-like macromolecular chains in the inner side,[79,80] the idea of using polymer brushes inside nanopores as controllable gates rose.[81,82] Approaches are versatile: different pore substrates (flexible membranes, metal surfaces and their combination), various gates (polymer brushes and hydrogels of different chemical nature) and several control mechanisms (external stimuli, single molecule recognition or electric current) have been applied, and are documented in several reviews.[83,84,85,86]

The NPC inspired new innovations in biosensing. Membrane proteins, bare solid pores, and pores with various coatings were tested with the aim of creating a sensor that could control the translocation of, and at the same time sequence one DNA strand, label-free, in real time and without damaging the structure.[87,88] Similarly, EMILSSON *et al.* gated proteins through gold nanopores coated with PEG brushes, monitored optically *via* refractometric techniques.[89] While they collapsed the PEG brushes (and opened the pores) with a suitable PEG antibody by single-molecule recognition, external stimuli-controlled gates inside gold coated nanopores (*e.g.* opened upon temperature changes) are yet to be tested with proteins. PNIPAM is a particularly interesting building block for thermoresponsive gates inside nanopores. With an LCST of 32 °C, it could easily open and close pores in a controlled manner by swelling and collapsing. Models have confirmed that gating solutes through nanopores using PNIPAM gates is indeed possible.[90] Additionally, PNIPAM brushes served as gates inside porous poly(ethylene) (PE)[90] and poly(ethylene therephtalate) (PET) membranes[91]. However, those flexible membranes deformed upon reswelling of the PNIPAM layers in their pores.[90] Pores in rigid substrates show reduced changes in geometry when exposed to an external stimuli (*e.g.* enhanced temperature).[84] Regardless of substrate, surface-initiated polymerizations provide a powerful tool for the synthesis of polymer brushes. Corresponding techniques are discussed in the following section.

2.3. The Synthesis of Polymer Brushes

Polymer brushes covalently bound to a surface can be synthesized in two ways: "grafting-from" and "grafting-to". In grafting-to techniques, the polymer contains anchor sites that bind to the desired surface. The polymerization occurs in solution prior to the surface attachment. In the grafting from approach, a suitable polymerization initiator is attached to the surface and then polymer chains are grown from there. Grafting-to allows for extensive analysis of the polymer before attaching it to the surface. In contrast, analysis of grafted-from polymers requires either degrafting or surface sensitive techniques. The pre-synthesized polymers used in the grafting-to approach are siginificantly larger than small initiator molecules, so grafting-to typically yields lower grafting density.[92] Inside nanopores, confinement on the pore walls might cause even lower grafting density when grafting-to.

Monodisperse polymer chains, *i.e.* a highly controlled polymerization, are desired. Uncontrolled termination and transfer reactions in common free radical polymerizations (FRP) lead to broad dispersities, and the number of side reactions and termination events increase with the amount of radicals. The development of controlled radical polymerization (CRP) enabled the synthesis of low dispersity polymers with various architectures and predictable molecular weight. In CRP, a nonreactive (so-called "dormant") species competes with the active radical. Ideally, the equilibrium between these states is shifted towards the dormant side to diminish undesired side reactions. Two main strategies exist for forming the dormant species: it can be a stabilized as a nonreactive radical as in nitroxide-mediated polymerization (NMP),[93] or reversibly deactivated through a suitable transfer agent as in reversible addition fragmentation chain transfer (RAFT)[94] and atom-transfer radical polymerization (ATRP)[95]. In ATRP, commercially available transition metal complexes form the transfer agents, whereas RAFT agents require individual preparation. ATRP was the technique used in this project and is hence described in detail in the following subsection.

2.3.1. Atom Transfer Radical Polymerization

In 1995, MATYJASZEWSKI and WANG developed copper mediated ATRP.[96] The initiator is provided as a halogenated organic molecule (R-X). Transition metal complexes with two available oxidation states and a free coordination position (*e.g.* a suitable Cu^I complex) serve as transfer agents,[97] which aid switching between the activated (radical, R·) and deactivated (R-X) species. The counterion of the positive XCu^I/L catalyst depends on the catalytic system used and the solvent.[98] During initiation of the polymerization, R-X is activated *via* oxidation of the complex ($Cu^I X/L_n$ to $Cu^{II} X_2/L_n$) and forms a radical. The rate of R-X activation by Cu^I is referred to as the activation rate constant (k_{act}).

The radical then propagates, consuming monomer until it is deactivated (rate constant: k_{deact}) by the addition of X. X is provided by the complex ($Cu^{II}X_2/L_n$), which is simultaneously reduced back to Cu^IX/L_n. The key point in this reaction is its reversibility. The redox reactions reform the reactive radical chain and the chain propagates further (rate constant: k_p), until it is deactivated again. Since the equilibrium favours the deactivated species, the radical concentration is drastically reduced compared to FRP. Also, termination reactions (rate constant: k_t) caused by radical combination are less likely to occur. The corresponding reaction equation is shown in Figure 2.4. The reaction kinetics are influence by k_{act} and k_{deact}, summarized by the reaction constant for atom transfer radical polymerization (K_{ATRP}) (Equation 2.5).

$$K_{ATRP} = \frac{k_{act}}{k_{deact}} \tag{2.5}$$
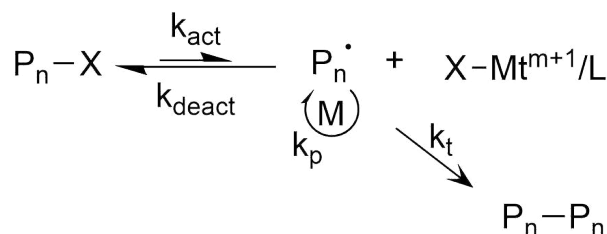
Scheme 2.4.: General reaction equation for ATRP.

Further development allowed for *in-situ* activators generated by electron transfer ATRP (AGET ATRP).[99] An oxidatively stable Cu^{II} species is initially provided, then transformed into its reactive Cu^I counterpart upon reaction with a suitable reducing agent (*e.g.* tin(II) 2-ethylhexanoate ($Sn(EH)_2$), hydrazine, phenol, glucose or ascorbic acid).[100,101] This simplifies the procedure since purification of the instable Cu^I is avoided. Highly reactive reducing agents are required to avoid long initiation periods. In contrast, reducing agents of lower reactivity are desired for activators regenerated by electron transfer ATRP (ARGET-ATRP). This technique reduces the catalyst concentation to below 100 ppm. Besides lowering the environmental impact, it eliminates the need for catalyst removal from the final product.[102] ARGET-ATRP remains successful in the presence of limited oxygen,[103] in aqueous systems,[104] and in non-deoxygenated reaction mixtures.[105] As ARGET-ATRP has become applicable to a broader audience countless derivations have followed, including surface-initiated activators regenerated by electron transfer ATRP.[106,107,107] Here, the initiator is self-assembled prior to "grafting from" polymerization.[105]

For surface-initiated reactions, it is particularly challenging to predict the necessary reaction conditions for a desired polymer chain length, even setting aside complex architectures and block copolymers. Several parameters influence K_{ATRP}: the catalyst,[98]

ligand and monomer,[95] their concentration,[105] solvent polarity,[108] and reaction temperature,[109] and pressure.[110] Ideal parameters must be found for individual systems – particularly for reactions on surfaces. A similar system to that investigated in this study (a PNIPAM-*co*-MBAM network) has been investigated previously.[89] EMILSSON *et al.* used SI-ARGET-ATRP to synthesize PNIPAM brushes from gold surfaces in a 1:1 MeOH/water mixture. CuBr$_2$ and *N,N,N',N'',N''*-pentamethyldiethylenetriamine (PMDETA) formed the catalytic species, and a disulfide self-assembled on gold provided the initiator. The authors investigated the reaction kinetics *in-situ* using SPR, an elegant surface-sensitive technique that is described in detail in the following subsection.

2.4. Surface Sensitive Analysis

2.4.1. Surface Plasmon Resonance (SPR)

Fundamentals of SPR

SPR occurs at the interface between a metal and a dielectric. When irradiated at wavelengths in the IR region, the conductive electrons close to the metal surface begin to oscillate. This oscillation can be regarded as an electromagnetic wave propagating along the metal surface. The term SPR was first mentioned together with a theoretic description of the phenomenon in 1902.[111] While MAIER[112] and HOMOLA[113] explain the fundamental theory of SPR in detail, only the most relevant aspects are described herein.

Metals typically reflect light of λ up to the visible region. In the UV-region, band electrons of noble metals such as gold and silver undergo electronic transitions, *i.e.* UV-light is absorbed. A complex dielectric function, $\epsilon(\omega)$ (representing the relative light permittivity of a material), describes these phenomena. The real part of $\epsilon(\omega)$ represents the energy stored in the material ($Re(\epsilon) > 0$ for dielectrics; $Re(\epsilon) < 0$ for metals). The imaginary part corresponds to losses, thus is always positive (the overall energy cannot increase). The MAXWELL equations build the basics for $\epsilon(\omega)$.[114]

An important variable in the theory of SPR is the propagation constant β. In a Cartesian coordinate system with a z-axis perpendicular to the metal surface, β describes the propagation along the metal surface (*i.e.* in x-direction). For the propagation of surface plasmon (SP)s at the simplest geometry (a flat interface between metal and dielectric) the dispersion relation shown in Equation 2.6 is valid. There, k_0 is the wavevector of the propagating light wave in vacuum, and ϵ_1 and ϵ_2 are the dielectric constants for the dielectric and metal layer, respectively, representing their light permittivity. The relation

between β the refractive index (n) is shown in Equation 2.8.

Light can only excite SP if its wavevector matches β_{SP}. Since β_{SP} at a metal-dielectric interface is larger than the wavenumber of light in a dielectric, direct excitation of SPs upon light irradiation at a smooth metal surface is impossible. Instead, special configurations increase the wavevector of light and hence enable the excitation of SPss: a prism coupler, where the light is guided through a high n prism prior to hitting the metal surface. Two different prism configurations were developed by OTTO and KRETSCHMANN.[115,116] The light path in a typical SPR instrument with a KRETSCHMANN configuration is shown in Figure 2.5.
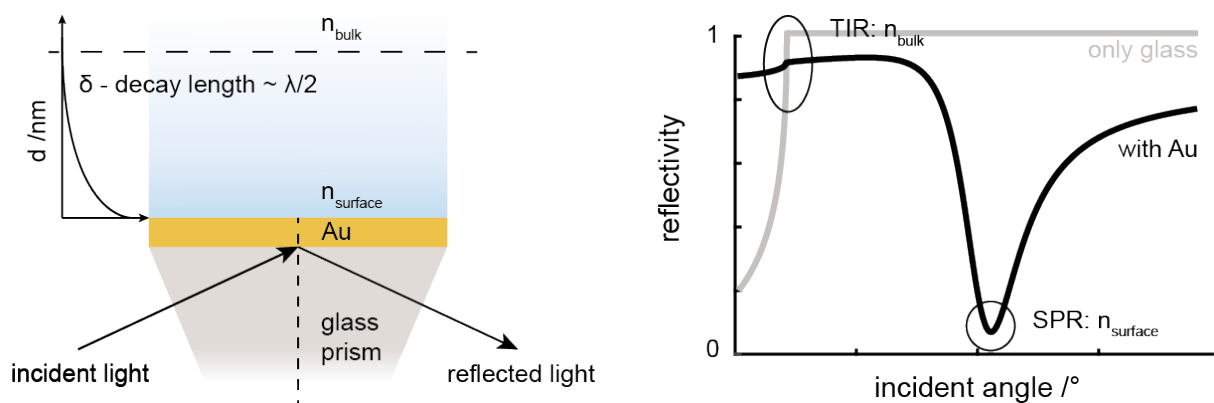
SPs are excited only if the matching condition (Equation 2.7) is fulfilled, where θ is the angle of incidence for the light beam, n_P the refractive index of the prism and λ the wavelength of the incident light. The real part of β depends on n of the dielectric in close proximity to the metal surface (n in Equation 2.8). Changes in θ at which SPs are excited (θ_{SPR}) correspond to changes in n of the liquid close to the surface. Therefore, SPR belongs in the category of refractometric analysis. The evanescent wave propagates along the metal-dielectric surface, and decays exponentially in the z-direction. The thickness of the layer that is probed by the light depends on λ of the incident light. This so-called penetration depth is defined as the distance from the surface at which the intensity of the evanescent wave decayed to $\frac{1}{e}$, where e is the base of the natural logarithm. While SPR is most sensitive close to the surface, n changes within a depth of $100\,\text{nm}$ to $600\,\text{nm}$ can generally be detected.[112,113]

$$\beta = k_0 \sqrt{\frac{\epsilon_1 * \epsilon_2}{\epsilon_1 + \epsilon_2}} \tag{2.6}$$

$$Re[\beta] = \frac{2\pi}{\lambda} * n_P * sin(\theta) \tag{2.7}$$
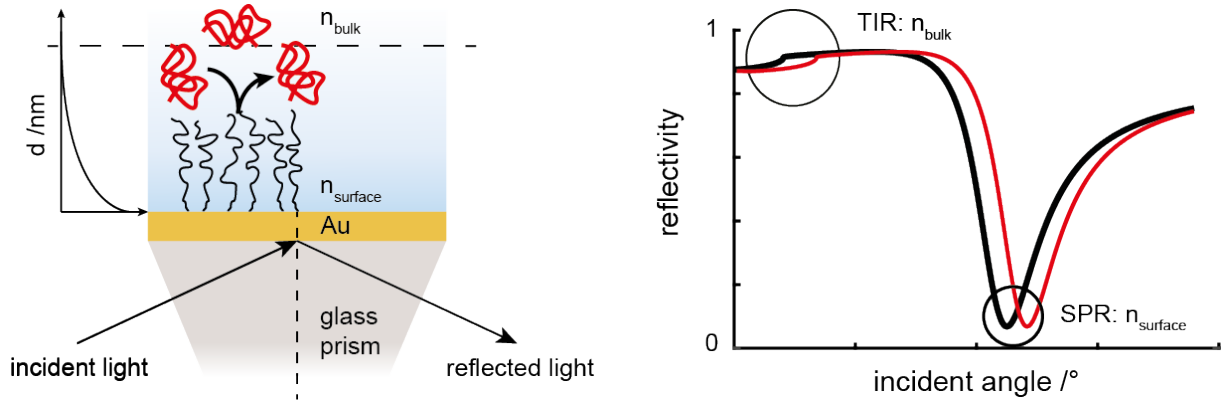
$$n = \frac{1}{k_0} * Re[\beta] \tag{2.8}$$

Figure 2.5.: Light path in an SPR instrument with a prism in KRETSCHMANN configuration (left hand side).[116] Incident light of a certain angle excites SPs, visible as a minimum at θ_{SPR} in the reflection spectrum of the gold surface (right hand side).

SPR is a powerful tool for the analysis of biological interactions.[117] If the metal surface (typically gold) is functionalized with suitable ligands, binding of targets is detectable as a change in n_{surf}. Similarly, polymers attached to metal surfaces result in a change of n_{surf}. The position of θ_{SPR} includes information about n and the layer thickness of the polymer. If n is known, which is usually the case for a dry polymer, the layer thickness can be determined by modelling the reflection spectrum obtained from measurements in ambient air, *e.g.* with FRESNEL models.[118,119] In addition to the layer thickness in the dry state, the heights of polymeric layers in solvents provide valuable information. However, the n of solvated polymers approaches that of the solvent, *i.e.* it undergoes a decrease in water (n_{H_2O}=1.33). Since the position of θ_{SPR} depends on both, n and layer thickness, an exact n value is essential to obtain correct polymer heights. It has been demonstrated that simply estimating the n for a swollen polymer layer (*i.e.* using literature values that were measured for polymers in solution) causes major inaccuracies in the obtained layer thicknesses.[120] Fortunately, SCHOCH *et al.* developed a powerful technique to obtain more accurate heights *via* SPR, which will be described in the following paragraph.[120]

The Non-Interacting Probe Method

This method is based on the fact that the polymeric layer occupies a certain amount of the total volume sense by SPR. SCHOCH *et al.* model the penetration depth (l_d), which represents the thickness of this sensed layer and is determined by the λ of the incident light. A "non-interacting probe" which neither binds to nor enters the polymer brush is then supplied an reveals the height of the layer that hinders the probe from entering (exclusion height). This approach is limited since the l_d depends on n too. If n of the polymer brush is significantly higher than the n of the solvent (*e.g.* above 1.4 for measurements in water where n=1.33), the exponential function of the SPR sensitivity shows a sharp bend at the interface of those two layers.[120] Low n layers include highly solvated polymer

Figure 2.6.: Light path in an SPR instrument with a prism in Kretschmann configuration during a non-interacting probe (*e.g.* BSA) injection (left hand side).[116] On the right hand side, an angular spectrum measured in pure PBS (black line) and one measured in BSA solution (red line) is depicted. Both θ_{SPR} and θ_{TIR} shift upon BSA injection.

brushes, *e.g.* PNIPAM brushes below the LCST. Above 32 ° °C PNIPAM undergoes a coil-to-globule transition. Upon collapsing, the n approaches 1.5 (n for dry PNIPAM).[121]

Fortunately, the non-interacting probe method was further developed by Emilsson *et al.* to apply to a broader range of n.[122] The described method is still based on a non-interacting probe (*e.g.* bovine serum albumine (BSA)). Angular spectra in both BSA solution and pure phosphate buffered saline (PBS) are recorded. Fresnel models (based on Snell's law) enable a comparison of those two spectra. Pairs of n and the brush height that model the spectrum of PNIPAM in pure PBS accurately are obtained. θ_{SPR} responds to n changes induced by BSA. Changes in θ_{TIR} upon BSA injection reveal n of the probe in the solution according to Equation 2.9 (see Figure 2.6). Thereby, any changes in θ_{SPR} caused by changes in the bulk solution (*e.g.* temperature, pH and concentration variations) are excluded prior to modelling the spectra obtained from measurements in BSA solution in the same manner as before for the spectra recorded in pure PBS. Again, a certain number of n and brush height pairs is obtained. Those n and brush height values are then plotted for all modelled spectra. Since changes in the bulk solution were taken into account previously, the intersection of the n and brush height pairs yields a distinct value for both. Thereby, n and the height of the layer that BSA does not enter are obtained, which is referred to as the "exclusion height".

$$\Delta n_{TIR} = n_{BSA} - n_{PBS} \tag{2.9}$$

SPR on Patterned Gold Surfaces

The extinction spectrum of a short-range nanopore array on a gold surfaces shows several characteristic features (Figure 2.7). Below 500 nm, gold strongly absorbs light, hence

any features corresponding to plasmon excitation in this region are hidden.[123] At higher λ, a maximum and minimum ("peak" and "dip") are typically observed in the excitation spectrum (highlighted in Figure 2.7).[124] Even though the exact phenomena that cause those features remain unknown, both correspond to plasmon excitation and are hence n-dependent. Any change in n_{surf} on the surface or inside the pores causes simultaneous changes in the position of peak and dip, respectively.[123] Previous studies demonstrated that the dip position is more sensitive to changes of n_{surf} inside the pores, and the peak to changes on the top surface.[125] XIONG *et al.* reported that the dip behaves like a localized plasmon confined to the pores, while the peak resembles SPR on the top gold surface.[126] However, as both are connected, no quantitative conclusions are possible. Nevertheless, monitoring n_{surf} changes is particularly valuable in protein gating. Protein binding to the silica nanowell bottom causes an n increase compared to pure PBS. If the proteins approach the surface below the penetration depth of the SPR wave, the peak and dip positions change. In contrast, both remain constant if a polymeric layer hinders them from entering the pores and approaching the surface. Protein translocation inside nanopores can thus be distinguished from a closed pore.[20]

Thermoresponsive behaviour of PNIPAM is visible on patterned surfaces since the n_{surf} changes – just as on flat gold surfaces. The optical techniques described here can be supported by another analytical technique based on acoustics: QCM-D.
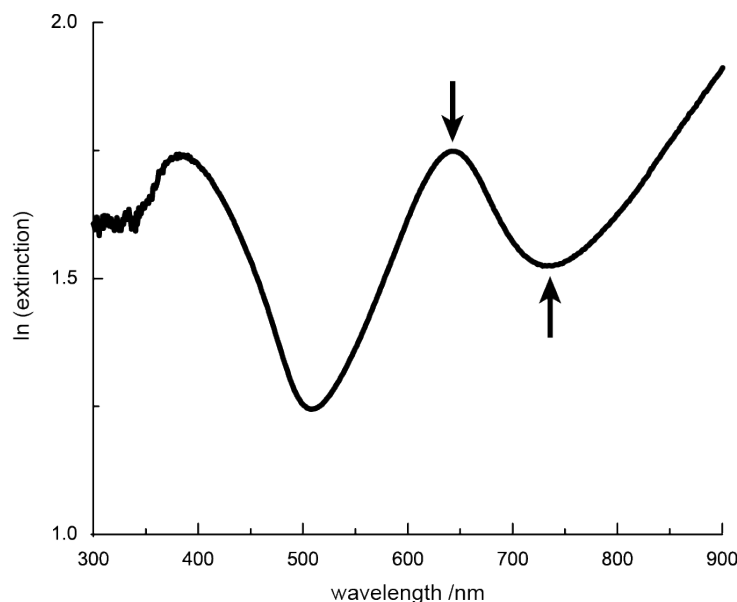
Figure 2.7.: Typical extinction spectrum of a polymer coated nanopore array on a gold surface, measured in transmission mode. Characteristic "peak" (extinction maximum) and "dip" (extinction minimum) are highlighted.

2.4.2. Quartz Crystal Microbalance

In this section, QCM-D is briefly summarized, focusing on the analysis of polymer brushes. Work by JOHANNSMANN[127] and VOINOVA[128] can be referred to for a more in-depth description.
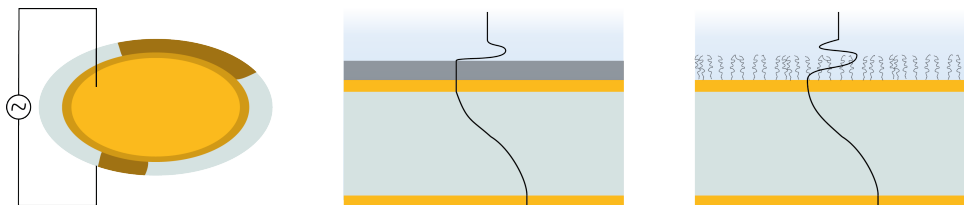
Figure 2.8.: From left to right: schematic of a gold coated converse piezoelectric QCM-D crystal. When a current is applied, the crystal oscillates and a standing wave is formed on the surface. The resonance frequency and energy dissipation of the amplitude depend on mass and viscoelastic properties of the layer close to the surface.

The basic element in a quartz crystal microbalance (QCM) instrument is a piezoelectric quartz crystal in the form of a thin disc. Shape changes in piezoelectric materials cause a potential difference, which can be measured. Equally, applying voltage to a converse piezoelectric crystal alters the shape. In QCM, the quartz crystal is sandwiched between two electrodes and excited by applying voltage, followed by a disconnection of the driving AC that leads to a characteristic oscillation at the resonance frequency (f_R) ($\approx 5\,\mathrm{MHz}$ for a bare crystal). SAUERBREY observed that adding mass on top of that crystal changes f_R according to Equation 2.10, where Δf is the f_R difference between the bare crystal and one with adsorbed mass, C is the constant for the quartz crystal ($17.7\,\mathrm{ng\,cm^{-2}\,Hz}$ for a 5 MHz crystal) and n is the overtone number.[127] Hence, changes in mass can be directly obtained from the frequency responses. However, this equation holds under certain restrictions only:

  i The film must be rigidly adsorbed.

 ii The mass must be evenly distributed on the relevant crystal surface.

iii Only a small mass is adsorbed compared to the mass of the crystal.

$$\Delta f = -\frac{C}{n} * \Delta m \tag{2.10}$$

Originally, the use of QCM was limited to investigations of adsorption processes from the gas phase to the quartz crystal.[129] Inspired by the observation that the oscillation is not dampened completely in liquid media,[130] several technological advances developed. In modern QCM devices, odd numbered overtones can be electronically excited (up to the 15th harmonic). Higher f_R (*i.e.* higher overtone numbers) dissipate energy faster in

viscous media, *i.e.* analysis is confined, but more precise, closer to the surface.[129]

Another valuable development was QCM-D. The SAUERBREY equation has limitations that prevent its use for soft films such as polymer layers, adsorbed proteins and hydrogels: whereas a rigid layer simply follows the oscillation of the crystal that it is adsorbed to, a viscoelastic material shows complex fluid behavior. The viscosity (η) of hydrogels consists of a real part (η') and an imaginary part (η"). The first describes the ideal-elastic part, while the latter resembles viscous behavior corresponding to rearrangements inside the polymer network – and hence energy losses. These losses dampen the oscillation in QCM, resulting in an underestimation of Δm using the SAUERBREY equation. Applying QCM to quantitative analysis of surface adsorption effects is also more complicated for soft films, since a direct calculation of adsorbed m from the observed Δf is not possible. However, for viscoelastic films, the energy dissipation contains valuable information that can be measured in QCM-D. The mathematical background, history and important applications of this development are well reviewed by SAKAI.[131] Briefly, the electric circuit is cut off for a short time, and the period necessary for the oscillation amplitude to diminish is measured as energy dissipation (D) of the signal. Changes in f_R and D are measured in 0.3-0.5 s intervals, allowing for *in-situ* observation of ad- and desorption phenomena, and changes in the rigidity of the adsorbed film. Whereas f_R of the oscillators (the crystals) depends mainly on the adsorbed m, D is related to the viscoelastic properties of the adsorbent. A higher D (*i.e.* a faster decrease in f_R) indicates an highly viscoelastic adsorbed film, and *vice versa*. This technique is especially valuable for investigating soft films, such as protein adlayers, polymer coatings and hydrogels.[132] However, for measurements in solution the "solvation-effect" causes overestimations of the adsorbed mass (m).[133] Since QCM is essentially a nanoscale balance (in contrast to optical instruments such as SPR), the adsorbed solvent causes additional changes in f_R and D. This is usually accounted for by measuring a bare sensor in parallel and subtracting the signal. While models may provide further information on the viscoelastic properties of the attached layers,[134,135] this goes beyond the scope of this work. Instead, interesting informations that can be gathered from monitoring the thermoresponsive behaviour of PNIPAM brushes and networks *in-situ* by QCM-D is emphasized.[136] In combination with thickness measurements obtained from SPR *via* the non-interacting probe method, this method provides information about changes in viscoelasticity and adsorbed mass upon temperature increase.

3. Aim and Motivation

Thermoresponsive polymers grafted to gold nanopore walls provide a promising approach towards controlled protein gating. Inspired by the NPC, the polymers act as a general gate, *i.e.* ideally they could gate any macromolecule. Trapping proteins from blood in the pores can be monitored by SPR, and the proteins further analysed for *e.g.* disease treatment after releasing them again.[122] PNIPAM with an LCST of 32 °C is a promising thermo-controllable gate material. Crosslinking PNIPAM brushes would adapt the LCST, pore diameter, and thus permeability of PNIPAM gates for specific biomacromolecules. While the thermoresponsive behaviour of PNIPAM brushes has been intensely investigated, detailed studies on their crosslinked counterparts are rare. Crosslinking was reported to alter the LCST of PNIPAM brushes,[6] and the swelling behaviour of bulk PNIPAM hydrogels;[65] but, a study how it affects the characteristic temperature dependent swelling and collapsing behaviour of surface-attached PNIPAM networks is missing. The aim of this work was to investigate the influence of crosslinking on the thermoresponsive behaviour of PNIPAM brushes. Knowing the exact layer thicknesses in both states is important if such networks are to gate protein translocation in nanopores. Therefore, the previously described non-interacting probe method was applied in this work to obtain exclusion heights of the crosslinked gels *via* SPR. Those heights revealed the swell:collapse ratio. Various comonomer ratios and two different crosslinking strategies were investigated. With the aim of preparing an *ex-situ* gel that crosslinks upon irradiation with UV-light, *N*-isopropyl acrylamide (NIPAM)-modified benzophenone was copolymerized with NIPAM. In contrast, a second comonomer – a bisacrylamide – should yield crosslinked brushes *in-situ*. Both copolymers were prepared on gold surfaces *via* SI-ARGET-ATRP. The obtained layers on flat gold surfaces were characterized with FT-IR spectroscopy, XPS, SPR and QCM-D measurements. Polymers were also grafted from nanopore containing gold sensors. The behaviour of dissolved proteins on sensor tethered PNIPAM networks was monitored *via* refractometric measurements in transmission mode. All corresponding results are shown and discussed in the following chapter.

4. Results and Discussion

This chapter is separated into two sections, the first pertaining to the *in-situ* PNIPAM-co-MBAM network, and the second a shorter section dedicated to PNIPAM-co-NBPAM. Since the copolymers were prepared in a similar manner, the procedure is only discussed once. Further details concerning concentrations, reaction conditions, and chemicals used are given in chapter 5.

4.1. SPR Heights

Three different thicknesses were measured for the polymer brush networks: dry, collapsed and swollen heights. Dry heights were obtained from measurements in air, while swollen and collapsed heights were both measured in PBS, at 25 °C and 35 °C, respectively. The heights were obtained using the non-interacting probe method, for which 35 kDa PEG provided a suitable, non-interacting probe. This is indicated by a linear relationship between SPR and total internal reflection (TIR) angle shifts upon probe injection (spectra shown in Figure A.4, Figure A.5 for PNIPAM-co-MBAM and in Figure A.6 and Figure A.3 for PNIPAM-co-NBPAM, respectively).

4.2. PNIPAM-co-MBAM

PNIPAM copolymers with MBAM were prepared *via* SI-ARGET-ATRP (Scheme 4.2). The influence of solvent, ratio of reducing agent to catalyst and crosslinker concentration on the reaction kinetics was investigated. The results obtained are discussed in the following subsections.

4.2.1. Initiator SAM

Prior to polymerization, gold surfaces were functionalized with the initiator ω-mercaptoundecyl bromoisobutyrate (Scheme 4.1). SAMs were obtained, and the dry height measured as 2 nm using SPR, in agreement with literature values.[62]
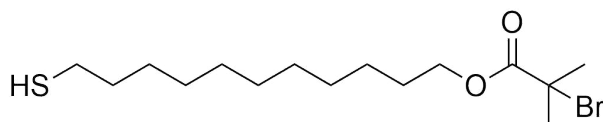

Scheme 4.1: Chemical structure of the initiator ω-mercaptoundecyl bromoisobutyrate.

4.2.2. SI-ARGET-ATRP

The SI-ARGET-ATRP was conducted following a previously reported procedure,[122] but using standard SCHLENK line techniques. $CuBr_2$ and the ligand PMDETA formed the transfer agent. To avoid previously observed interactions between the acrylate monomers and the catalyst,[137] the ligand was used in large excess. The blue solution vanished upon addition of the reducing agent ascorbic acid, indicating the reduction of blue $[Br_2Cu^{II}/PMDETA]$ to colorless $[BrCu^{I}/PMDETA]$ (Scheme 4.3). The polymerization was stopped by expose to air. The presence of the polymeric layer on top of the gold surfaces was varified by FT-IR. Corresponding results are shown and discusses in the following subsection.
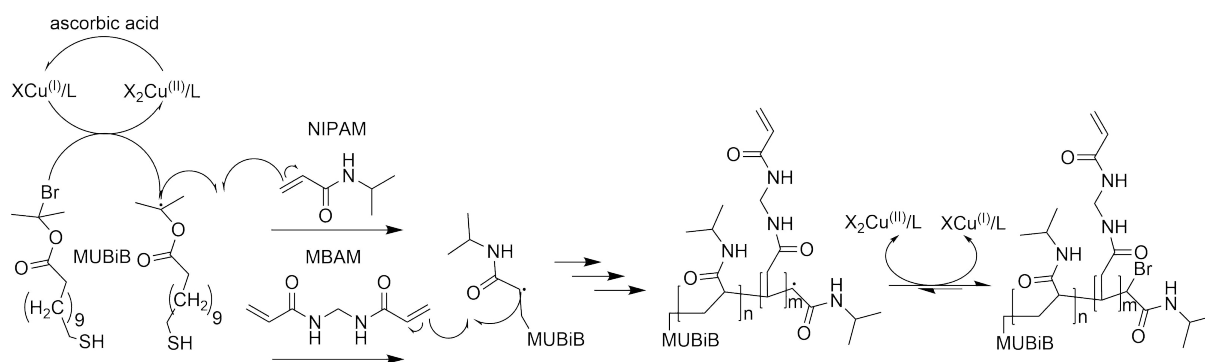
Scheme 4.2: A solution of the monomer NIPAM, crosslinker MBAM and complex $[Br_2Cu^{II}/PMDETA]$ in MeOH or MeOH/mQ mixtures is added to a ω-mercaptoundecyl bromoisobutyrate functionalized gold surface. Upon addition of ascorbic acid, the formed $[BrCu^{I}/PMDETA]$ initiates the SI-ATRP to yield PNIPAM-co-MBAM.
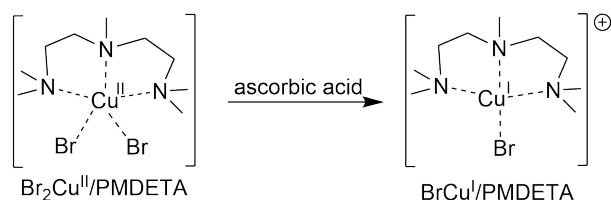
Scheme 4.3: Ascorbic acid reduces the deactivated $[Br_2Cu^{II}/PMDETA]$ to the activated $[BrCu^{I}/PMDETA]$ catalyst. Noteworthy, one equivalent (eq) ascorbic acid reduces two eq of the catalyst.

FT-IR Results

The FT-IR spectrum of a PNIPAM brush without crosslinker is shown in Figure 4.1. A detailed FT-IR study of PNIPAM was reported by MUNK *et al.* who carefully assigned every band,[138] an overview of which is given in Table A.1. The spectra of corresponding gels containing MBAM do not show any additional modes (Figure A.17), but we are certain that the networks do contain crosslinker due to experiments detailed in subsection 4.2.4 and subsection 4.2.5. Increasing the amount of crosslinker in the gels appears to decrease

the overall spectra intensity. This indicates that thinner layers are obtained on the sensed surface areas, and hence supports the quantitative results obtained from SPR experiments. PNIPAM-co-MBAM gels attached to gold are highly prone to water absorption from ambient air as indicated by broad bands at $\tilde{\nu}=3100\,\mathrm{cm}^{-1}-3700\,\mathrm{cm}^{-1}$ and $1640\,\mathrm{cm}^{-1}-1650\,\mathrm{cm}^{-1}$ in the FT-IR spectra. Previous studies involving a PNIPAM-co-MBAM system with 10 mol% MBAM showed that the hydrophilicity increases if the gel is attached to a hydrophilic surface,[63] *e.g.* gold surfaces.[139]
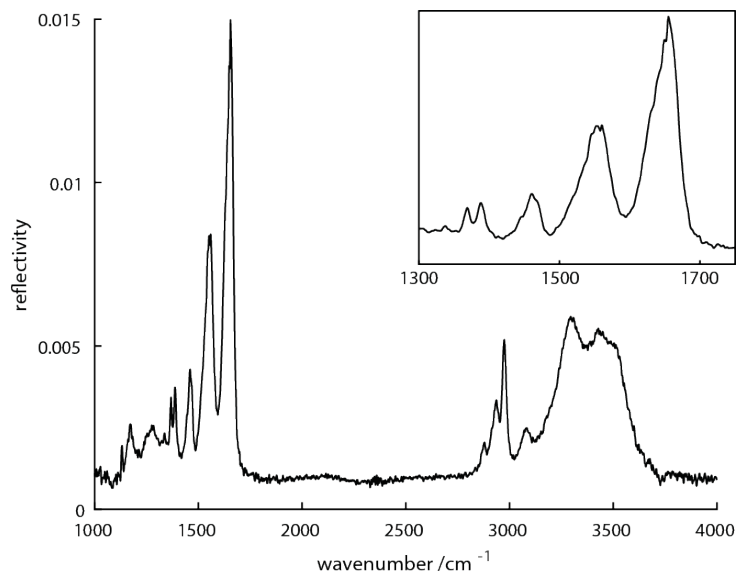

Figure 4.1.: FT-IR spectrum of PNIPAM brushes on gold, measured in reflection mode. A zoom of the region between $\tilde{\nu}=1300\,\mathrm{cm}^{-1}$ and $1700\,\mathrm{cm}^{-1}$ is shown in the top right corner.

The Ascorbic Acid to Catalyst Ratio

In SI-ARGET-ATRP, the ratio of ascorbic acid to the catalyst determines the ratio of activated [BrCu$^{\mathrm{I}}$/PMDETA] to [Br$_2$Cu$^{\mathrm{II}}$/PMDETA], and thereby highly impacts the reaction kinetics. Ascorbic acid provides two electrons to reduce 2 [Br$_2$Cu$^{\mathrm{II}}$/PMDETA] to 2 [BrCu$^{\mathrm{I}}$/PMDETA] (Scheme 4.4). The deactivated Cu$^{\mathrm{II}}$ species decreases the reaction speed and increases control. A highly controlled polymerization is important to homogeneously distribute crosslinker throughout the polymeric layer. It was previously reported that a ratio of Cu$^{\mathrm{I}}$:Cu$^{\mathrm{II}}$=0.8:0.2 results in low dispersity polymers, indicating high control.[100,105] We thus employed 0.4 eq of ascorbic acid with respect to CuBr$_2$ (*i.e.* 0.8 stoichiometric eq), which due to an immediate reduction would give the ratio Cu$^{\mathrm{I}}$:Cu$^{\mathrm{II}}$=0.8:0.2 at the onset of the reaction. However, no or extremely thin polymeric layers were obtained after 4 h (0.48 M): 5 nm dry height in MeOH, 2 nm in DMSO (including a 2 nm initiator layer). This could have occurred due to oxidation of the catalyst, for which the solution would be adding excessive reducing agents to restore the activated XCu$^{\mathrm{I}}$/L species.[105] However, slow regeneration of XCu$^{\mathrm{I}}$/L is crucial for controlled reactions, which is impos-

sible using a fast acting reducing agent like ascorbic acid.[100]

Ascorbic acid does show several advantages compared slower reacting reducing agents such as tin(II) 2-ethylhexanoate, hydrazine and phenols: it is harmless, environmentally friendly, and oxidatively stable.[137] Fortunately, a continuous ascorbic acid supply to the reaction solution was reported to yield polymers of low dispersity – indicating high control.[140] Adding 0.4 eq with respect to $CuBr_2$ (0.8 stoichiometric eq.) initially and continuously supplying $0.49\,nmol\,min^{-1}$ ascorbic acid to an initial reaction volume of 10 mL for 4 h in MeOH did yield a thicker polymer network (13 nm), and so these conditions were pursued for all further reactions in MeOH. Interestingly, even though a blue color was expected after the initial ascorbic acid addition, the reaction mixture appeared colorless immediately. This indicates that no $[Br_2Cu^{II}/PMDETA]$ remains. Thus, to further control the reaction, even less ascorbic acid could be added in future.
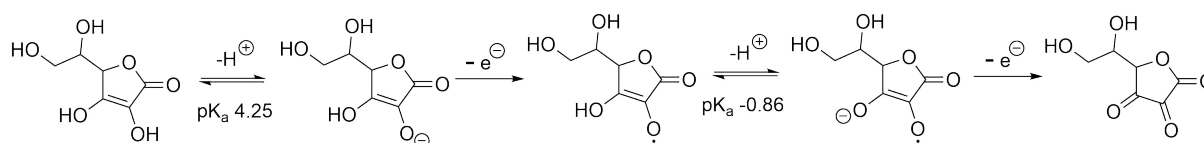
Scheme 4.4: At physiological pH-values, ascorbic acid appears in its deprotonated form, as shown on the left hand side. It may act as a reducing agent twice, and is reported to form several products upon further oxidation by exposure to oxygen.[141]

In-situ monitoring of a SI-ARGET-ATRP in QCM-D

SI-ARGET-ATRP of PNIPAM-co-$MBAM_1$ at 0.48 M in MeOH was investigated *in-situ*. The QCM-D experiment followed a procedure described in the literature.[142] An incomplete reaction mixture without any reducing agent (*i.e.* no activated Cu^I complex) was supplied to a gold QCM-D sensor coated with a ω-mercaptoundecyl bromoisobutyrate self-assembled monolayer (SAM). The flow was then switched to a complete reaction mixture containing 0.8 eq of ascorbic acid. The SI-ARGET-ATRP initiation is clearly visible as a sudden decrease of f_R and simultaneous increase of D in Figure 4.2. The chains propagate, as a slow decrease in f_R indicates. After 180 min both f_R and D flatten out, *i.e.* the SI-ARGET-ATRP stops, most likely due to termination reactions. As expected from preliminary experiments, this reaction seems to be rather slow. A higher monomer concentration or different solvent might solve this.
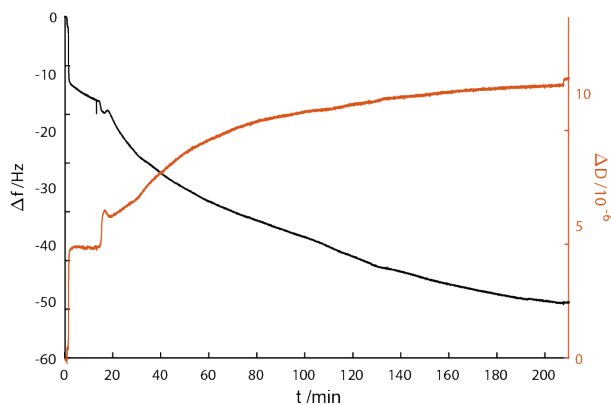
Figure 4.2.: SI-ARGET-ATRP of PNIPAM-co-MBAM$_1$ (0.48 M) was monitored *in-situ* in a QCM-D experiment. A sudden increase after 2 min indicates the polymerization initiation. Afterwards, the curves flatten out, indicating a slow propagation followed by a complete termination at $\approx$180 min.

The Solvent in SI-ARGET-ATRP

Solvents play a key role in ATRP. They affect the catalyst activity, *i.e.* its efficiency to cleave the R-X bond, and hence K_{ATRP}.[143] Since K_{ATRP} is very low for (meth)acrylates,[144] adding water to organic solvents accelerates SI-ARGET-ATRP for these monomers.[145,146,147] PNIPAM-co-MBAM gels were prepared in a 2:1 MeOH:milipore water (mQ) mixture (0.48 M), and the kinetics investigated (Figure 4.3). The polymer network dry height increased linearly for the first hour, then levelled out. A similar trend was observed for the collapsed heights of the same samples. This indicates a loss of reactive R-X groups, caused by chain termination or dissociation reactions. Similar kinetics were reported in literature previously.[122] The reaction in MeOH:mQ=2:1 mixtures yielded non-reproducible gel heights. The obtained gel layers after 30 min had an average dry height of 33.4 nm $\pm$ 8.5 nm − *i.e.* the dry height varied by 25 % across five repeats. For ATRP in aqueous solvents, accelerating the reaction comes at the cost of control: higher K_{ATRP} means a higher radical concentration and hence more termination events. Moreover, hydrolysis of the R–X bond, and dissociation of the ligand or halide from the Cu^{II} species in water also reduce control, especially in ARGET-ATRP where low catalyst concentrations are used.[104]
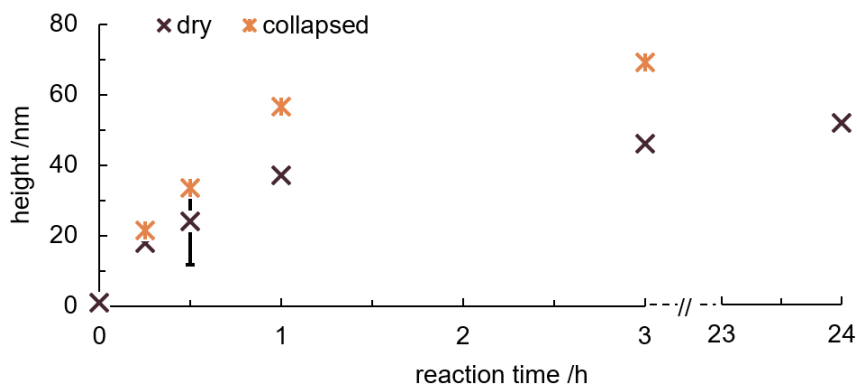
Figure 4.3.: Kinetic plot for SI-ARGET-ATRP of NIPAM (0.48 M and 1 mol% MBAM in mQ:MeOH=1:2. The dry height increases linearly in the first hour, and levels out afterwards, with an 8.5 nm deviation for a 30 min reaction. The collapsed height shows a similar trend.

To increase control in the reaction, water was removed as a solvent. Preliminary experiments and the *in-situ* QCM-D experiment in MeOH proceeded so slowly that brush heights for the herein desired application gating 80 nm diameter pores could only be obtained after several days. The catalyst and monomer concentrations were thus doubled (0.96 M). The kinetic plot is shown in Figure 4.4. After just 1 h, dry heights of 29 nm were measured. The increased concentration aptly counters the decreased reactivity expected upon removing mQ as a solvent. Additionally, the heights of gels prepapred in MeOH are more reliable: networks prepared in 24 h had an average dry height of 26.5 nm ± 0.5 nm on samples prepared in different batches. More control was established by using only an organic solvent.
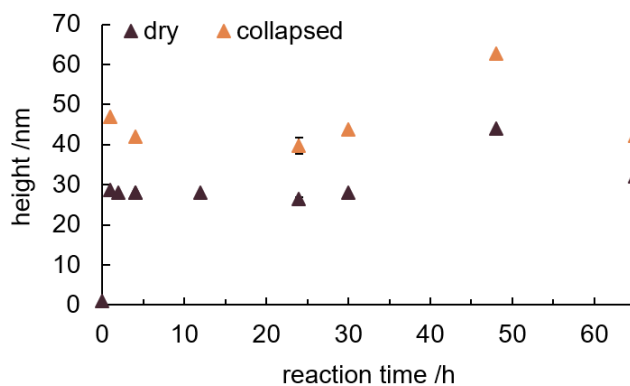
Figure 4.4.: Kinetic plot for SI-ARGET-ATRP of NIPAM (0.96 M) and 1 mol% MBAM in MeOH. Gels prepared in 24 h show a height deviation of only 0.5 nm.

The Concentration of the Crosslinker MBAM

In further experiments, the amount of MBAM was varied between 0 mol% and 10 mol% with respect to total monomer concentration. Increasing the MBAM concentration gradually reduced the dry thickness, as shown in Figure 4.5. This was observed previously in

SI-ATRP of crosslinked PAAM brushes, and an interaction between monomer and catalyst suspected as the reason.[62] Importantly, the opposite was true in photo-iniferter polymerization of PAAM and MBAM,[51] reactions which lack a catalyst.[148] In SI-ARGET-ATRP only ppm of the catalytic species is used, so the reactions are highly sensitive to catalyst poisoning.
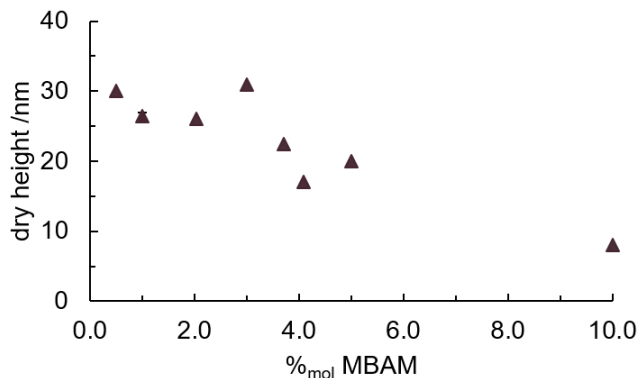
Figure 4.5.: Kinetic plot for the SI-ARGET-ATRP of NIPAM and varied amounts of MBAM (0 mol% to 10 mol%) in MeOH.

In conclusion, a highly controlled reaction with a linearly increasing growth curve could not be established for the preparation of PNIPAM-co-MBAM. Reactions in MeOH clearly showed more control compared to those in mQ:MeOH mixtures.

4.2.3. Termination

Termination was observed in all reactions investigated. The thicknesses of network layers obtained from SI-ARGET-ATRP in mQ:MeOH=1:2 (0.48 M) and *in-situ* in MeOH (0.48 M) levelled out after 1 h and 1.5 h, respectively. Increasing the concentration in MeOH (0.96 M) lead to complete termination after 1 h, but yielded polymeric layers of similar heights. These results show that water-mediated dissociation events of the catalyst or R-X cannot be the only reason for termination. ZHOU *et al.* assign terminations in SI-ARGET-ATRP models to what they call "migration termination":[149] if a radical is formed in close proximity to an existing radical, they combine and terminate. Normally in ATRP the catalyst concentration (and hence the radical concentration) is so low that such termination reactions are unlikely. However, on surfaces slow diffusion of the catalyst leads to more active radicals due to a loss of the deactivated Cu^{II} species. Migration termination is thus a serious problem in SI-ARGET-ATRP, as observed in our experiments.

4.2.4. QCM-D Results

The crosslinker MBAM was expected to alter the swelling behaviour of PNIPAM brushes. SI-ARGET-ATRP of PNIPAM-co-MBAM was carried out in MeOH (0.96 M) for 24 h (the

conditions that give the lowest deviation in dry height). We varied the reaction crosslinker content between 0 mol% and 10 mol% with respect to the total monomer content. In this section, we examine the changes in the viscoelastic properties and mass of several gel samples upon temperature variations using QCM-D. Temperatures varying from 22 °C up to 40 °C were investigated in PBS at pH 7.5. Since the density and viscosity of PBS are temperature dependent, a bare gold sensor was always measured in parallel and any signal subtracted later.

In Figure 4.6, the results for PNIPAM-co-MBAM gels are compared, with MBAM contents of 0.5 mol%, 1 mol%, 3 mol% and 10 mol% are compared. Upon a temperature increase from 25 °C to 35 °C, f_R increases, *i.e.* the mass attached to the sensor decreases – as the polymer expels water. A reduction in D indicates more rigid layers. As expected, PNIPAM-co-MBAM$_{0.5}$, PNIPAM-co-MBAM$_1$ and PNIPAM-co-MBAM$_3$ expel water and rigidify upon a temperature increase from 25 °C to 35 °C. The volume phase transition happens over a temperature range, *i.e.* is a discontinuous transition, and this range broadens with increasing MBAM content. Whereas PNIPAM-co-MBAM$_{0.5}$ and PNIPAM-co-MBAM$_1$ is fully collapsed at ≈27 °C, PNIPAM-co-MBAM$_3$ expels water up to a temperature of ≈30 °C. Moreover, the thermoresponse gradually decreases with increasing MBAM content, up to a point when it vanishes completely for PNIPAM-co-MBAM$_4$ (Figure A.10). Upon a temperature decrease back to 22 °C all networks belatedly reswell to the same extent as before the first collapse. Although only one swell and collapse cycle is depicted in Figure 4.6, up to three temperature variation cycles were applied and revealed a fully reversible swelling behaviour regardless of crosslinker content (Figure A.12–A.15). While only qualitative conclusions can be drawn from the QCM-D experiments, SPR quantitatively reveals the heights of PNIPAM-co-MBAM at a certain temperature as described in the following subsection.
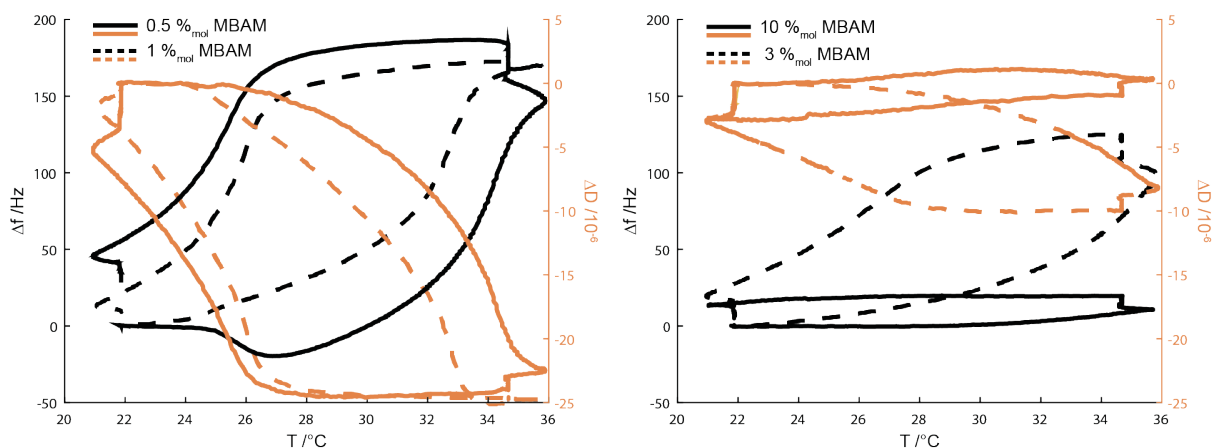
Figure 4.6.: Left: comparison of PNIPAM-co-MBAM$_{0.5}$ (solid line) and PNIPAM-co-MBAM$_1$ (dashed line). Right: comparison of PNIPAM-co-MBAM$_3$ (dashed line) and PNIPAM-co-MBAM$_{10}$ (solid line). The recorded shifts for f_R are depicted in black and correspond to the left y-axis, whereas changes in D are shown on the right y-axis and in orange. Increasing the amount of crosslinker causes less of response to temperature changes up to a point at 10 mol% where the thermoresponsive behaviour vanishes completely.

4.2.5. SPR Results

To analyse the thermoresponsive behaviour of PNIPAM-co-MBAM, SPR measurements were carried out. As shown in Figure 4.7, the swell:collapse ratio decreases with increasing crosslinker content, up to a point between 5 mol% and 10 mol% where the thermoresponsive behaviour is almost lost. While the height in the collapsed state (at temperatures >32 °C) remains constant, the thickness of the swollen layer decreases with increasing MBAM (Figure A.1 & A.2). Literature reports of various crosslinked polymer brushes noted the same behaviour when they compared dry and swollen heights.[6,53,65] This occurs as crosslinking polymer brushes introduces confinement and hinders them from swelling. Moreover, the PNIPAM-co-MBAM network seems to crosslink with a random efficiency (*i.e.* the amount of in the product incorporated crosslinker varies between surfaces), indicated by a deviation of 0.4 in the swell:collapse ratio of two gels prepared with 1 mol% MBAM.
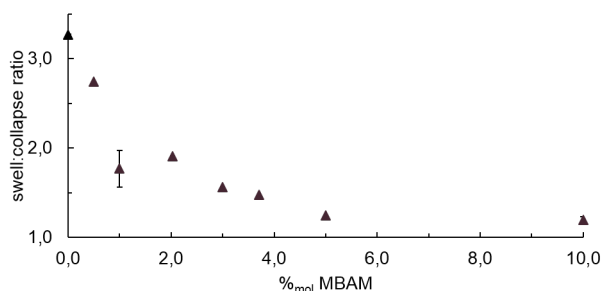
Figure 4.7.: Swell:collapse ratio for PNIPAM-co-MBAM gels with various amounts of MBAM (0 % to 10 %) in the reaction feed, all prepared in MeOH (0.96 M, 24 h).

The reaction time was previously reported to alter the swell:collapse ratio for PNIPAM brushes prepared in a MeOH:mQ=1:1 solvent.[122] Longer reaction times yielded brushes with a lower swelling factor (and thicker dry heights). The same trend was observed 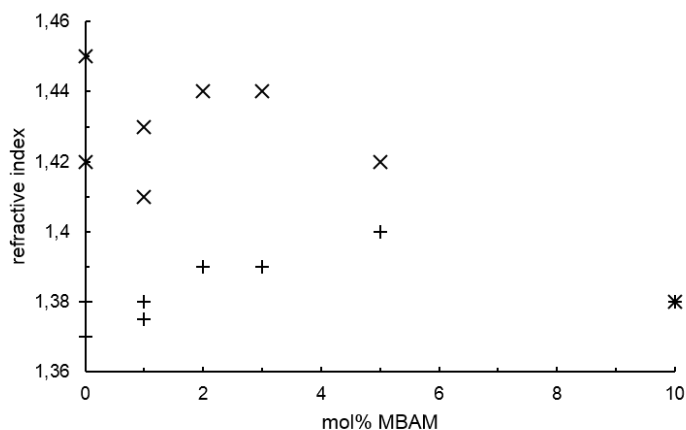here for PNIPAM-co-MBAM networks prepared in MeOH:mQ=2:1 (Figure 4.8, right side). The deviation of dry heights for PNIPAM-co-MBAM networks prepared in 30 min is again quite high (27 %). The swelling behaviour of a non-crosslinked PNIPAM brush was in the range of that of PNIPAM-co-MBAM$_1$ prepared in 30 min. This is either a direct consequence of the deviation in dry heights (see Figure 4.3), or caused by a random reactivity (with respect to the supplied crosslinker amount in the reaction feed) and hence crosslinking efficiency of MBAM. In contrast, the swell:collapse ratio is independent of the reaction time for reactions carried out in pure MeOH with 1 mol% MBAM (Figure 4.8). Moreover, it only deviates 12 % for samples prepared under the same conditions. However, for reactions in MeOH the concentration of catalyst and monomers was double of the reactions carried out in MeOH:mQ=2:1. Besides the solvent, this could also have an effect on the swelling behaviour.
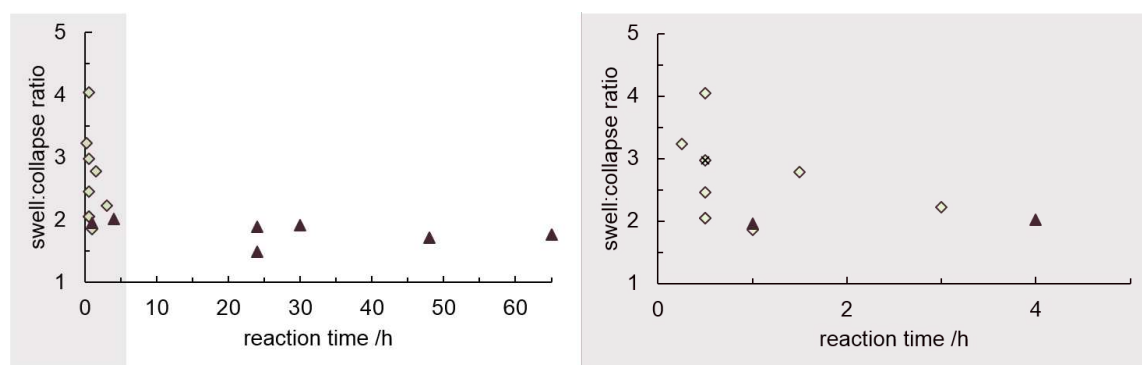
Figure 4.8.: Left: Swell:collapse ratio of PNIPAM-co-MBAM$_1$ networks with reaction time. For SI-ARGET-ATRP in MeOH (▲, 0.96 M), the reaction time has no influence. Right: A zoom for shorter reaction times emphasizes the high variation for samples prepared in a MeOH:mQ=2:1 mixuture (◊, 0.48 M). For comparison, the result for a non-crosslinked brush (MeOH:mQ=2:1, 0.48 M, 30 min) is depicted (x, right side).

With the non-interacting probe method, both height and n of the polymeric layer can be determined. The reaction time does not influence the n of PNIPAM-co-MBAM$_1$ prepared in MeOH:mQ=2:1 (Figure A.8) or MeOH (Figure A.7). Neither is there an obvious link between crosslinker content and n of swollen or collapsed PNIPAM-co-MBAM prepared in MeOH (0.96 M, 24 h, Figure 4.9).

Figure 4.9.: n for PNIPAM-co-MBAM with varying crosslinker content prepared in MeOH (0.96 M, 24 h) shows no trend. x represent the n measured at 35 °C and + those obtained from spectra at 25 °C.

Longer SPR experiments revealed a constant wet height for PNIPAM-co-MBAM$_1$ (prepared in MeOH:mQ=2:1, 0.48 M, and in MeOH, 0.98 M, respectively) probed in 20 min intervals up to a time of 5 h under a continuous flow of PBS (20 µL/ min, pH 7.5) at 25 °C. In contrast, the wet height of uncrosslinked PNIPAM brushes in a similar experiment decreased by 10 nm (from 100 nm to 90 nm) in 1 h. KO *et al.* reported degrafting of highly stretched polymer brushes in aqueous solution previously, and suspected swelling induced tensile forces acting on the brushes as the cause.[150]

4.2.6. PNIPAM-co-MBAM Inside Nanopores
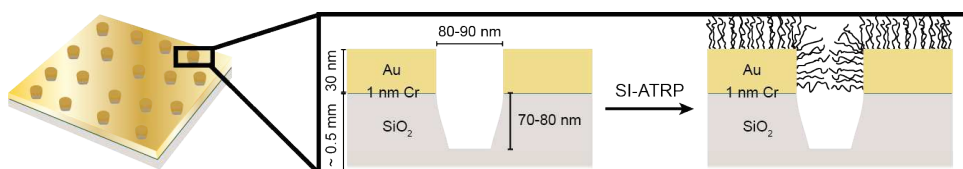
Figure 4.10.: Schematic of a typcial nanowell. Polymer layers grown on the gold surfaces *via* SI-ARGET-ATRP form thermocontrollable gates inside the pores.

To test PNIPAM-co-MBAM as a gate towards protein translocation, it was polymerized (MeOH, 0.96 M, 24 h) on gold surfaces containing an array of nanowells of diameter 80–90 nm and deepness 70–80 nm (Figure 4.10). Nanopores with gold surfaces enable growth of a polymer layer inside the pores to from thermoresponsive gates, while growth on the top surface protects the gold from unspecific protein binding. Thinner layers are expected on the walls compared to the top gold surface since confinement hinders diffusion of reactants into the pores. [BrCu^{I}/PMDETA] must diffuse into the pore to initiate the polymerization. As it may first encounter initiator molecules on the top surface to react with, the concentration of active catalyst in the pores may be particularly low. ALEM *et*

al. observed that PNIPAM brush layers inside 80 nm diameter pores swell 8x less than brushes on the top surface of the same sensor.[91] Increasing reaction times enhanced this effect due to the top polymeric layer beginning to cover the pores. Since the polymer brush height on the pore walls is lower than on the top gold surface, finding appropriate reaction conditions to produce a successful gate is challenging. PNIPAM-co-MBAM$_1$ on SPR slides showed a swell:collapse factor of ≈ 2, thus a range of gel heights was expected to enable thermo-controlled gating.

Investigating Interactions between Proteins and PNIPAM in QCM-D

Prior to conducting gating experiments, any potential interactions between the protein lysozyme (LZ) and PNIPAM-co-MBAM were investigated using QCM-D (Figure 4.11). First, the temperature of three sensors: a bare gold surface, PNIPAM, and PNIPAM-co-MBAM$_1$, in PBS (pH 7.5) was increased from 25 °C to 35 °C to confirm the thermoresponsive behaviour. A simultaneous rise in f$_R$ and drop in D were as expected. Then, a solution of LZ (50 µg mL^{-1}) in PBS (pH 7.5) was supplied at both temperatures. The f$_R$ of the bare reference sensor immediately decreased while D increased, as LZ formed a soft layer on the gold surface. In contrast, both PNIPAM and PNIPAM-co-MBAM$_1$ did neither show any change in signal at room temperature nor at 35 °C. Thus, any (ir)reversible interactions were excluded for both swollen and collapsed layers on flat substrates.
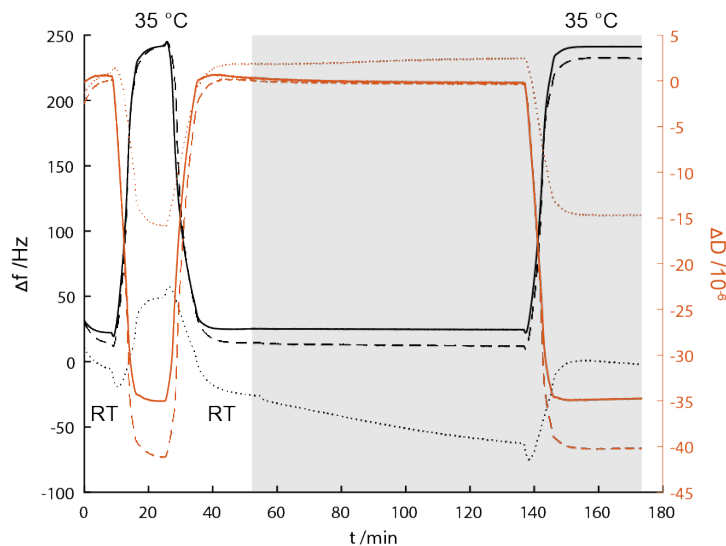
Figure 4.11.: Interactions of LZ with a bare gold sensor (dotted line), PNIPAM brushes (dashed line) and PNIPAM-co-MBAM$_1$ networks (continuous line) were tested in a QCM-D experiment. The temperature was increased from 25 °C to 35 °C. Then, LZ was supplied at 25 °C and 35 °C as indicated by a grey background. LZ binds only to the bare gold reference, indicated by a drop in f$_R$.

Insplorion Experiments with LZ on PNIPAM-co-MBAM$_1$

LZ did not interact with PNIPAM or PNIPAM-co-MBAM$_1$ on flat substrates, so similar experiments were performed with nanowell sensors. In a typical experiment, positional shifts in peak and dip (originating from changes in n) were monitored under continuous flow in transmission mode using an instrument called Insplorion. The response of PNIPAM-co-MBAM$_1$ measured in PBS (pH 7.5) is shown in Figure 4.12. Upon increasing the temperature from 25 °C to 35 °C, both peak and dip redshifted, indicating an increasing n caused by the collapse of the layer. When the heating was switched off, both peak and dip returned to the previous baseline – $i.e.$ the network re-swelled to the same extent. Supplying LZ at 25 °C had no effect, since PNIPAM-co-MBAM$_1$ prevents the protein from entering the pore or binding to the gold surface. No leakage was observed even after 30 min. This is important as it demonstrates that swollen PNIPAM-co-MBAM$_1$ gels inside pores form an impenetrable barrier for LZ. In contrast, when LZ was supplied at 35 °C (collapsed PNIPAM-co-MBAM$_1$) it clearly entered the pore, as the peak and dip both shifted significantly. At this pH, LZ shows a positive net charge and hence binds to the unprotected negatively charged silica well bottom. The 0.3 nm increase in the dip upon LZ binding inside the wells agrees with a control experiment (Figure A.9), in which LZ bound to open nanopores grafted with short 2 kDa PEG (the PEG prevents binding to the gold surface). Alongside the QCM-D results, this confirms that LZ is binding inside the pores rather than interacting with the surface-attached network.

Similar experiments using nanowell samples coated with PNIPAM-co-MBAM$_4$, PNIPAM-co-MBAM$_2$ and PNIPAM are discussed in the following subsections.
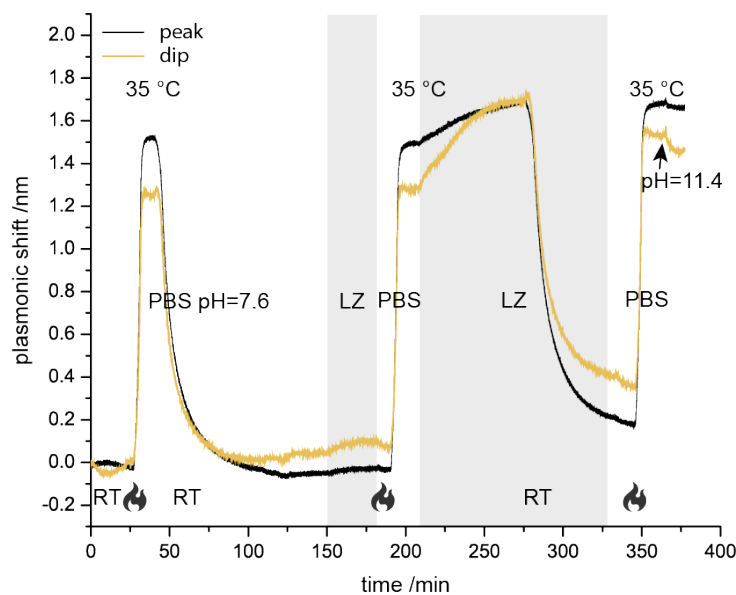
Figure 4.12.: LZ gating experiment on a nanowell sensor coated with PNIPAM-co-MBAM$_1$. 50 µL min^{-1} PBS (pH 7.5) was supplied continuously (white background), the temperature varied as indicated and a solution of LZ in PBS (50 µg mL^{-1}, pH 7.5) injected (grey background).

**Insplorion Results for the Swelling Behaviour**

PNIPAM-co-MBAM$_{3.7}$, PNIPAM-co-MBAM$_2$ and PNIPAM were grafted from nanowell and SPR sensors as described previously. Dry, swollen, and collapsed heights of PNIPAM-co-MBAM$_2$ were consistent with PNIPAM-co-MBAM$_1$ by SPR on smooth gold surfaces. However, the corresponsding nanowell samples (Figure 4.13 and Figure 4.12, respectively) displayed different behaviour: a temperature increase to 35 °C caused a +1.5 nm shift in the peak position for PNIPAM-co-MBAM$_1$, but only a +0.95 nm shift for PNIPAM-co-MBAM$_2$. This deviation may occur for several reasons. The grafting density between the two nanowell sensors could vary due to contamination or scratches on the gold surface. SPR and Insplorion results must also be distinguished; whereas the non-interacting probe method senses the exclusion height for a 35 kDa PEG probe, changes in n are measured in Insplorion. Additional crosslinker in the network might not significantly alter the swell:collapse factor, but will change n in the swollen state as shown in Figure 4.9. Finally, the polymerization kinetics differ between smooth and patterned gold surfaces: polymerizations inside nanopores slow down over time as diffusion inside becomes blocked by thicker polymer layers on top.[91] Moreover, interaction with MBAM are suspected to poison the catalyst.

The crosslinker content was then increased further. For PNIPAM-co-MBAM$_{3.7}$, the swell:collapse ratio was reduced compared to PNIPAM-co-MBAM$_1$ and PNIPAM-co-MBAM$_2$ (determined with the non-interacting probe method). This was confirmed by Insplorion by lower peak and dip shifts in PNIPAM-co-MBAM$_{3.7}$ (Figure 4.14). Interestingly, both peak and dip do not return back to the original baseline after heating to 35 °C then colling back to 25 °C, *i.e.* the network does not reswell to the same extent.

Finally, a PNIPAM brush containing no crosslinker was grafted from SPR and nanowell samples. By SPR, the PNIPAM brushes swelled by a factor of 3.2 compared to their collapsed state, giving a height 160 % that of PNIPAM-co-MBAM$_1$ or PNIPAM-co-MBAM$_2$ at 25 °C. By Insplorion, increasing the temperature to 35 °C caused a peak position shift of 3.6 nm (Figure 4.15). This larger shift upon collapsing is expected based on the swelling factor, as more PBS is expelled. The non-interacting probe method revealed that both, a higher n in the collapsed state and a lower n in the swollen state (Figure 4.9) lead to this huge peak shift. In summary, across these samples we observed that increasing the crosslinker content led to a decrease in the shift of the peak position. This supports our observations from SPR measurements.

LZ on Different PNIPAM-co-MBAM Copolymers in Insplorion

After collapsing and reswelling samples, LZ was injected first at 25 °C and then at 35 °C. While PNIPAM-co-MBAM$_1$ allows for thermo-controlled gating, other polymer brushes and networks act differently. The PNIPAM brushes were unable to prevent LZ from translocating inside the nanowells at 25 °C, even though their exclusion height in the swollen state was 119 nm (pore diameter: 80–90 nm, Figure 4.15). The dip position shifted by +0.25 nm as LZ bound to the silica support; note that the control experiment for LZ showed a shift of 0.3 nm. For PNIPAM-co-MBAM$_{3.7}$, LZ seems to enter the network at 25 °C (Figure 4.14). This is observed as a partially reversible shift of the dip: when LZ is supplied, the dip position increases by +0.4 nm, and decreases back to +0.2 nm. Upon a second and third LZ injection, fully reversible shifts were observed: first +0.2 nm, and then -0.2 nm when washed with PBS. Some LZ bound irreversibly during the first injection, but otherwise it entered the network or approached the surface reversibly. This behaviour is even more pronounced at 35 °C: the dip shifted beyond +1.1 nm. Washing with PBS at 35 °C decreased the shift to +0.9 nm in the dip, but this is significantly more than the expected shift of 0.3 nm from the control experiment. Hence, some interactions between LZ and PNIPAM-co-MBAM$_{3.7}$ are irreversible or the huge shift means it appears to be binding on the top surface too. Reversible interactions between PNIPAM-co-MBAM$_2$ and LZ were observed at 25 °C in both peak and dip (Figure 4.13). Further investigation could use fluorescence microscopy to reveal more details about protein movement inside the networks.
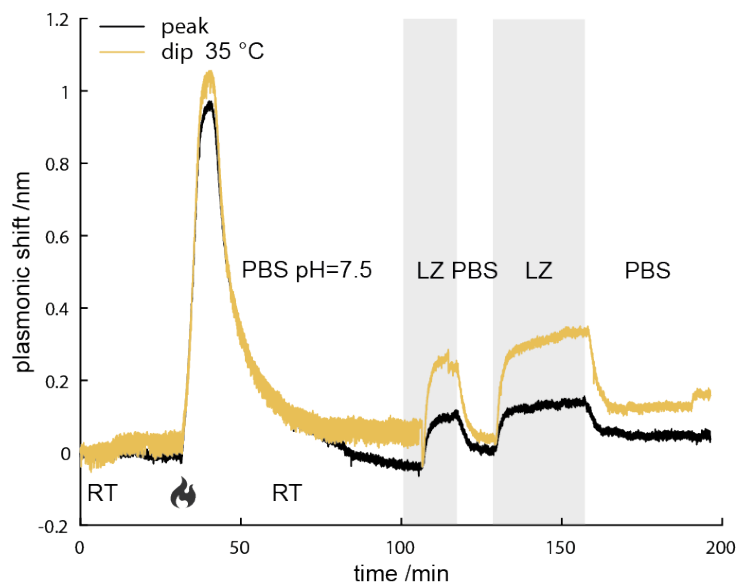
Figure 4.13.: LZ gating experiment on a nanowell sensor coated with PNIPAM-co-MBAM$_2$. 50 µL min^{-1} PBS (pH 7.5) was supplied continuously (white background), the temperature varied as indicated and a solution of LZ (50 µg mL^{-1}, pH 7.5) injected (grey background).

Figure 4.14.: LZ gating experiment on a nanowell sensor coated with PNIPAM-co-MBAM$_{3.7}$. $50\,\mu l\,min^{-1}$ PBS (pH 7.5) was supplied continuously (bright background), the temperature varied as indicated and a solution of LZ ($50\,\mu g\,mL^{-1}$, pH 7.5) injected (grey background).
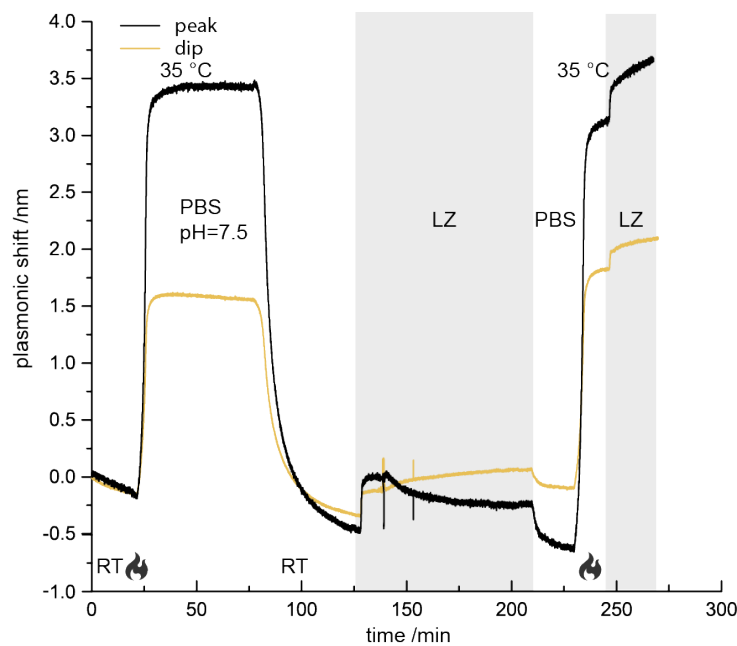
Figure 4.15.: LZ gating experiment on a nanowell sensor coated with PNIPAM. $50\,\mu L\,min^{-1}$ PBS (pH 7.5) was supplied continuously (white background), the temperature varied as indicated, and a solution of LZ in PBS ($50\,\mu g\,mL^{-1}$, pH 7.5) injected (grey background.

4.3. PNIPAM-co-NBPAM

PNIPAM brushes can be crosslinked *ex-situ* upon UV-irradiation if they contain a suitable comonomer, *e.g.* benzophenone.[151] The gels can then be directly compared to the parent brushes on the same surface, which eliminates sensing the effects of variables outside of crosslinking on the LCST, swelling behaviour, and dry thickness. If benzophenone was not incorporated in the polymer brush but provided in solution, a reduced crosslinking efficiency and brush shortening caused by backbiting (*i.e.* self-attack) and followed disproportionation was observed by CHRISTENSEN and coworkers.[152]

In this work, UV-light crosslinkable brushes, copolymers of NIPAM and a modified benzophenone, NBPAM, were prepared *via* SI-ARGET-ATRP. The results are presented in the following subsections.

4.3.1. SI-ARGET-ATRP

PNIPAM-co-NBPAM was prepared in a similar procedure to PNIPAM-co-MBAM (Scheme 4.5). As NBPAM is soluble in dioxane but not in MeOH or mQ and ascorbic acid not soluble in pure dioxane, SI-ARGET-ATRP was carried out in mQ:dioxane mixtures (1:1 and 1:4). In all reactions, a yellow precipitate formed upon the addition of mQ (most likely NBPAM, which appeard as a yellow powder). Nevertheless, SI-ARGET-ATRP did proceed under these conditions, as discussed in the following subsections.
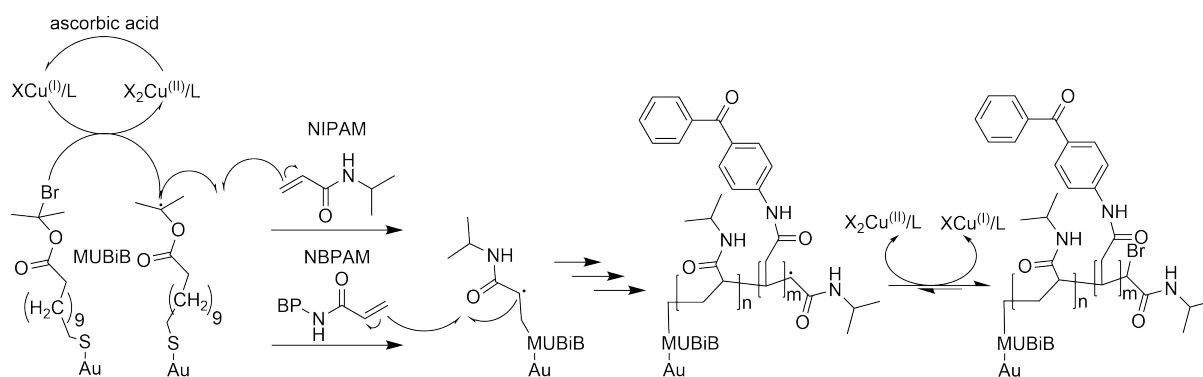
Scheme 4.5: A solution of NIPAM, NBPAM, and Br_2Cu^{II}/PMDETA in dioxane or dioxane/mQ mixtures was added to a ω-mercaptoundecyl bromoisobutyrate functionalized gold surface. Upon addition of ascorbic acid, the formed $BrCu^{I}$/PMDETA initiates the SI-ATRP towards PNIPAM-co-NBPAM.

4.3.2. FT-IR Results

The FT-IR spectrum of PNIPAM-co-NBPAM is shown in Figure 4.16. It contains an additional band at $\tilde{\nu}=1600\,cm^{-1}$ compared to the spectrum of PNIPAM (Figure 4.1), which corresponds to the C=C stretch of the aromatic rings in the crosslinker.[153] The characteristic $C=O_{benzophenone}$ at $\tilde{\nu}=1664\,cm^{-1}$[153] and the aromatic C=C deformation

expected at $\tilde{\nu}=3040\,\mathrm{cm}^{-1}$ are masked by the N-H and C=O bands of PNIPAM. To confirm the FT-IR results, XPS measurements to test NBPAM incorporation in the brushes were carried out. The obtained results are presented in the next subsection.
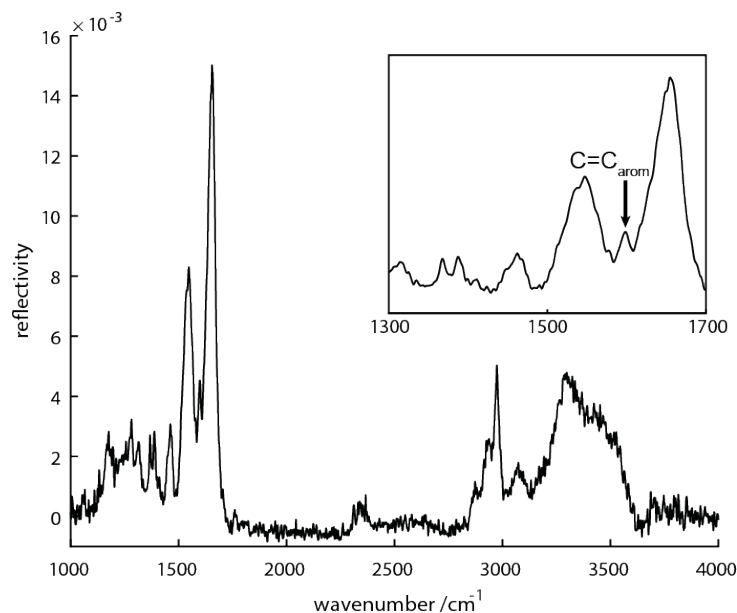
Figure 4.16.: FT-IR spectrum of PNIPAM-co-NBPAM brushes on gold, measured in reflection mode. A zoom of the region between $\tilde{\nu}=1300\,\mathrm{cm}^{-1}$ and $1700\,\mathrm{cm}^{-1}$ is shown in the top right corner. Compared to the spectrum obtained from PNIPAM, an additional mode at $\tilde{\nu}=1600\,\mathrm{cm}^{-1}$ corresponding to aromatic C=C stretch modes is highlighted.

4.3.3. XPS Results

PNIPAM and un-crosslinked PNIPAM-co-NBPAM brushes were analysed by XPS. The corresponding results are shown in Table 4.1. Si was detected in the PNIPAM-co-NBPAM sample, indicating scratches on the gold surface that revealed the underlying SiO_2 substrate. As expected, the sample with NBPAM contained less nitrogen than the PNIPAM brushes – further confirmation of inclusion of the crosslinker.

Table 4.1.: XPS results for PNIPAM-co-NBPAM$_2$ and PNIPAM, respectively.

| atom$_{\text{sample}}$	expected amount /%	observed amount /%
C_{PNIPAM}	75.0	76.14
O_{PNIPAM}	12.50	11.83
N_{PNIPAM}	12.50	12.01
$C_{\text{PNIPAM-co-NBPAM}}$	75.18	73.10
$O_{\text{PNIPAM-co-NBPAM}}$	12.46	15.06
$N_{\text{PNIPAM-co-NBPAM}}$	12.35	9.4

4.3.4. SPR Results

To determine dry, swollen and collapsed heights, SPR measurements were carried out on PNIPAM-co-NBPAM grafted from gold sensors. Swollen and collapsed heights were measured in PBS at 25 °C and 35 °C, respectively, with the non-interacting probe method (Table 4.2). 35 kDa PEG was used as the probe, and did not interact as indicated by a linear TIR vs SPR relationship (Figure A.3–A.6). A swollen height just 3 nm thicker than the collapsed height indicates that the PNIPAM-co-NBPAM brush is not thermoresponsive even before crosslinking. The aromatic moiety in NBPAM might cause hydrophobic brushes, *i.e.* prevent their swelling in aqueous media. To confirm this, PNIPAM brushes were prepared under the same conditions and investigated by QCM-D as discussed in the following subsection.

Table 4.2.: Obtained heights measured in air for PNIPAM-co-NBPAM prepared in the indicated solvent in 30 min.

mQ:dioxane ratio	dry height /nm	swollen height /nm	collapsed height /nm
1:1	31	–	–
1:1	23	19	16
1:4	15	–	–

4.3.5. QCM-D Results

To test the effect of NBPAM on the non-crosslinked brushes, PNIPAM was prepared under the same conditions. Without a significant influence of NBPAM, those brushes should show a similar swelling behaviour. PNIPAM brushes prepared under the same conditions were investigated by QCM-D (Figure 4.17). They expel far more PBS upon increasing the temperature to 35 °C than a PNIPAM-co-NBPAM$_1$ brush. This is indicated by a f$_R$ shift of 370 Hz for pure PNIPAM compared to 75 Hz for PNIPAM-co-NBPAM$_1$. With the obtained heights from SPR measurements, it can be concluded that the higher f$_R$ shifts are caused by more swollen PNIPAM brush layers at 25 °C (containing more PBS than PNIPAM-co-NBPAM$_1$, rather than less collapsed PNIPAM-co-NBPAM$_1$ layers at 35 °C. The benzophenone moiety with its two aromatic rings is highly hydrophobic. A 1 mol% benzophenone content is sufficient to hinder the chains from swelling: instead of extended brushes, physically crosslinked networks are formed in PBS (Figure 4.18).
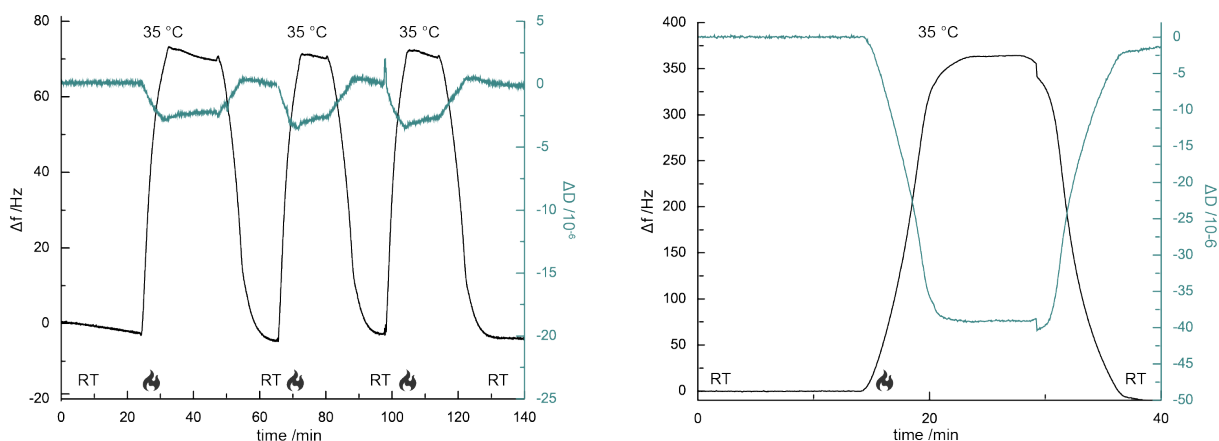
Figure 4.17.: QCM-D plots of PNIPAM-co-NBPAM$_1$ (left) and PNIPAM (right) prepared in a mQ:dioxane=1:1 mixture in 30 min. PNIPAM shows a f_R shift of 350 Hz compared to only 80 Hz for PNIPAM-co-NBPAM$_1$ upon a temperature increase, indicating a collapsed PNIPAM-co-NBPAM$_1$ layer already at temperature=25 °C.
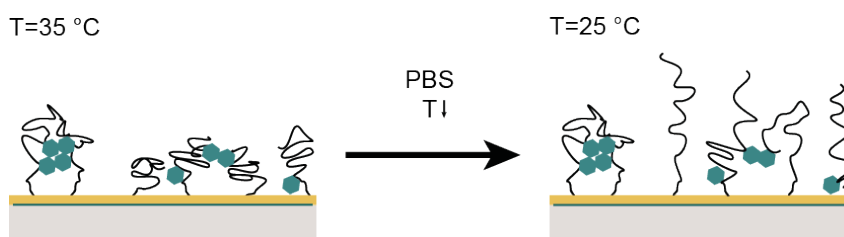
Figure 4.18.: The hydrophobic aromatic moieties in PNIPAM-co-NBPAM brushes form physical crosslinks in aqueous media. The blue hexagon represents NBPAM incorporated in PNIPAM brushes.

4.3.6. Crosslinking PNIPAM-co-NBPAM

Although the PNIPAM-co-NBPAM brushes were deemed non-thermoresponsive, the crosslinking was investigated to demonstrate the principle.

Crosslinking of NBPAM containing brushes was reported previously.[154] When irradiated with UV-light (λ=365 nm), benzophenone forms a radical. This radical abstracts an H atom from any C-H bond to form of two new radicals: C· and ·C-OH$_{benzophenone}$. Crosslinks between brushes are then formed *via* three possible radical combinations (Scheme 4.6): two benzophenone radicals form a pinacol, a benzophenone combines with a brush backbone C·, or two of the latter react with each other.

We irradiated PNIPAM-co-NBPAM brushes with UV-light (λ=365 nm) for 10-30 min. In QCM-D, the f_R shift observed upon a temperature increase remained the same as before irradiation, indicating either that crosslinking did not alter the thermoresponsive behaviour, or that the reaction did not occur. Considering that incorporated crosslinks typically decrease the swell:collapse factor of polymer brushes (non-crosslinked PNIPAM-co- NBPAM: swell:collapse factor=1.2), a thermo-induced volume phase transition that

remains low is not surprising. In the future, incorporating less NBPAM in the polymer brushes might increase the brush swelling at room temperature and thermoresponsive character of PNIPAM-co-NBPAM brushes and their crosslinked counterparts.
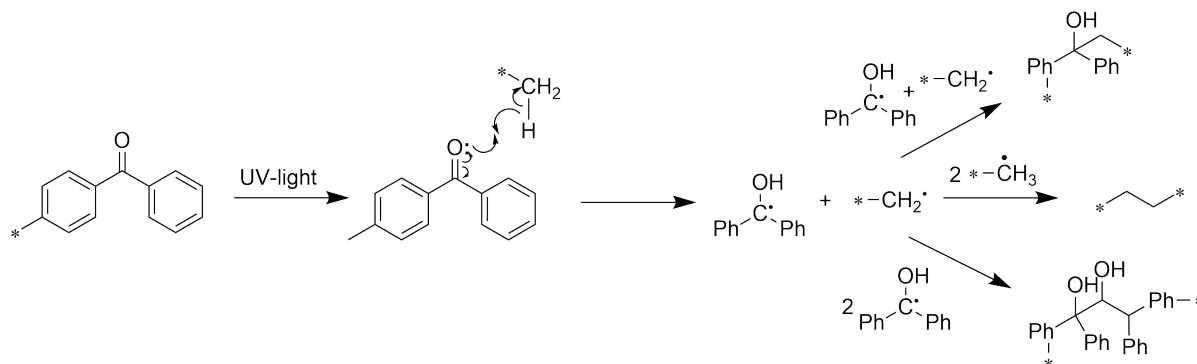
Scheme 4.6: Upon irradiation with UV-light, benzophenone forms radicals that may cleave any C-H bond of a brush backbone upon formation of another radical. Following crosslinking can occur *via* three different pathways.

4.4. Conclusion and Outlook

Two copolymers were grafted from gold surfaces. The thermoresponsive behaviour of *ex-situ* crosslinkable PNIPAM-co-NBPAM and *in-situ* crosslinked PNIPAM-co-MBAM was investigated.

The crosslinker MBAM clearly influenced the thermoresponsive behaviour of PNIPAM brushes. SPR and QCM-D experiments both confirmed that the characteristic swell:collapse ratio gradually decreases with increasing MBAM content in the reaction feed. This results from a decreased swelling at $25\,°C$ rather than higher collapsed heights. Additionally, the dry gel height remained constant with reaction time, but decreased with increasing MBAM in the reaction feed, suggesting that MBAM may poison the catalyst. Controlled ATRP was observed in MeOH, where polymers with low deviation in dry height were obtained; but polymerizations using a MeOH:mQ=2:1 solvent mixture were more uncontrolled, yielding products with a $25\,\%$ dry height deviation. In contrast to previous reports,[6] our PNIPAM copolymers all showed similar VPTTs in QCM-D.

The second crosslinker investigated, NBPAM, altered the thermoresponsive behaviour of PNIPAM as well, but not in the expected manner. Even prior to crosslinking the films did not swell due to the highly hydrophobic aromatic moieties in benzophenone.

Gating experiments carried out with the protein LZ and PNIPAM-co-MBAM grafted nanowell sensors were successful for gels containing $1\,mol\%$ MBAM. PNIPAM-co-MBAM$_1$ forms an impenetrable barrier for LZ at room temperature, all other investigated samples did allow LZ to enter the networks (PNIPAM-co-MBAM$_2$ and PNIPAM-co-MBAM$_{3.7}$) or even the pores (PNIPAM).

The polymerization procedure established in this work together with results on the thermoresponsive behaviour of PNIPAM-co-MBAM layers could inspire further applications in biosensors and other MFDs. Future work will initially focus on fluorescence microscopy experiments to confirm the behaviour observed by PNIPAM-co-MBAM$_1$. Afterwards, tests with full serum will provide a further step towards a successful protein trapping device based on thermocontrollable PNIPAM-co-MBAM gates.

5. Materials and Methods

5.1. Analytical Techniques

5.1.1. FT-IR

FT-IR spectra of SPR sensors were recorded (10 scans, $4\,cm^{-1}$ spectral resolution) in reflection mode on a PMA50 spectrometer (Bruker, Germany). Background spectra were collected by scanning a bare gold SPR sensor. Three spectra were measured for each sample on varied sensor surface positions and averaged.

5.1.2. QCM-D

Gold coated, circular QCM-D sensors with a diameter of $14\,mm$ and a f_R of $\approx 5\,MHz$ were purchased from QuartzPRO. Measurements were performed using a Q-Sense E4 instrument (Biolin Scientific) equipped with a peristaltic pump (Ismatec, Germany). *Ex-situ* coated gold crystals were mounted in the measurement chamber and flushed with PBS until a stable baseline was established. The introduced error from subtracting f_R and D of a parallel measured reference were determined as $\pm\,5\,Hz$ and $\pm\,5*10^{-6}$, respectively by mounting pure sensors in all three of the used flow cells (plot shown in Figure A.11). Those inaccuracies might be caused by small differences in temperature, flow rate or crystal mass.

5.1.3. SPR

SPR experiments were performed at the Chalmers Material Analysis Laboratory, CMAL. Gold coated SPR sensors were purchased from BioNavis. Slides with a gold thickness of $\approx 50\,nm$ were used for all SPR experiments. All SPR experiments were performed in a SPR Navi™ 220A instrument (BioNavis) equipped with four lasers (2x 670 nm, 785 nm and 980 nm). Dry heights were obtained by recording angular spectra of the respective sample in air and modelling them with FRESNEL models[155] using a software from RES-TEC (Winspall, Version 3.02). The used parameters are portrayed in Table 5.1. Experiments in solution were conducted in PBS with a flow rate of $20\,\mu L\,min^{-1}$. First, a stable baseline was established in the solvent. The non-interactive probe (35 kDa PEG or BSA at a concentration of $10\,mg/mL$ in PBS) was injected in serial mode for 7 min, with a 7 min rinse with the running buffer in between each injection.

layer	d /nm	n_{785nm}	κ_{785nm}	n_{670nm}	κ_{670nm}
silica/elastomer[122]	∞	1.5162	0	1.5020	0
Cr[122]	0.9	3.3225	3.6148	3.3105	3.4556
Au[156]	50	0.16088	5.0525	0.16194	3.9783
initiator	2	1.45	0	1.45	0
PNIPAM[121]	h	1.4973	0.0018745	1.5	0.0021271
air	∞	1.0003	0	1.0003	0

Table 5.1.: Used parameters for FRESNEL models of the recorded spectra in SPR experiments in air to obtain dry heights.

5.1.4. Insplorion

Refractometric measurement on nanowell sensors were carried out using an XNano instrument (Insplorion, Sweden). A peristaltic pump (Ismatec, Germany) pumped PBS (pH 7.5, $50\,\mu L/\min$) through a metallic flow cell that provided for resistive heating. Absorption spectra were recorded in transmission mode, the peak and dip position selected and changes monitored in a following continuous measurement. Protein solution were prepared in PBS (pH 7.5, $50\,\mu g\,mL^{-1}$).

5.1.5. XPS

XPS was performed on a PHI 5000 VersaProbe III Scanning XPS Microprobe (Ulvac-Phi, Japan) equipped with a monochromated Al X-ray source ($24.6\,W$, $45°$, measured range: 0-1486.6 eV). Any measured oxygen belonging to SiO_2 was compensated for. The oxygen amount corresponding to SiO_2 was calculated using the Si signal and subtracted from the total measured oxygen content to obtain the oxygen content in the polymeric layer.

5.2. Chemicals

All chemicals and proteins used were purchased from Sigma-Aldrich and used as received unless stated otherwise.

EtOH (99.5 %) was from Solveco, ammoniumhydroxide (25 % solution) from Fischer, NBPAM from Angene, SH-modified PEG (2 kDa) from Laysan Bio Inc., and ω-mercaptoun decyl bromoisobutyrate from ProChimia. Water was ASTM research grade TypeI ultra-filtered water (mQ water). Buffers were based on PBS tables (0.01 M phosphate, 0.13 M NaCl, pH=7.4). The polymerization solvents methanol (99.8 %) and DMSO (>99 %) were dried over 3 Å molecular sieves (Merck) and stored under N_2. NIPAM (99 %, Fischer) was recrystallized from hexane at $85\,°C$ and stored under N_2 afterwards. The proteins used in this study were BSA and LZ (obtained from white henegg, ThermoFisherScientific).

5.3. Experiments

5.3.1. Surface Cleaning

Prior to surface functionalization, QCM-D sensor crystals and SPR sensor surfaces were cleaned with piranha wash (H_2SO_4:H_2O_2 3:1 v/v) for 30 min, rinsed with mQ, then cleaned with TL1 wash (mQ:NH_3:H_2O_2 5:1:1 v/v, 80 °C) for 30 min. The nanowell sensors (pores of 80–90 nm diameter, 70–80 nm deepness) were kindly provided by J. ANDERSSON who prepared them following a previously reported procedure.[157] The Al_2O_3 layer was first removed in 0.01 M NaOH for 1 h, followed by cleaning in TL1 for 30 min. Finally, all sensors were rinsed with mQ and EtOH, then dried with N_2.

5.3.2. Surface Activation

Clean gold surfaces were placed in a petri dish containing a ω-mercaptoundecyl bromoisobutyrate solution (0.002 M in EtOH), sealed with parafilm, and shaken (50 rpm) for 16-24 h

5.3.3. SI-ARGET-ATRP

PNIPAM brushes and PNIPAM-co-MBAM gels were prepared under the same reaction conditions (Scheme 5.1). The amount of MBAM supplied in the monomer feed was varied between 0 mol% (for brushes) up to 10 mol%. Reactions were carried out using standard SCHLENK line techniques under an inert atmosphere of N_2. Unless stated otherwise a 10 mL reaction volume was used.
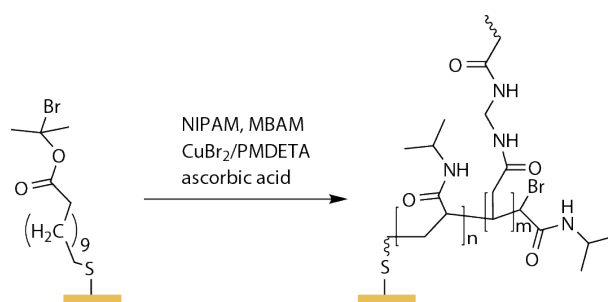
Scheme 5.1: SI-ARGET-ATRP of PNIPAM-co-MBAM.

SI-ATRP in an mQ/MeOH mixture

Reactions were carried out using standard SCHLENK line techniques under an inter atmosphere of N_2. Depending on the desired crosslinker content, varying amounts of both monomers were used according to Table 5.2. In one flask, monomers NIPAM (*e.g.* 0.5377 g, 0.48 M final c, 792 eq for PNIPAM-co-MBAM₁), MBAM (*e.g.* 7.4 mg,

0.004 75 M final c, 8 eq for PNIPAM-co-MBAM$_1$), and solvents mQ (2.7 mL) and MeOH (5.3 mL; mQ:MeOH=1:2 v/v) were added to inhibitor remover. The solution was degassed with N$_2$ for 5 min. In a second flask, CuBr$_2$ (1.4 mg, 0.0006 M final c, 1 eq) was added to PMDETA (13.6 µL, 0.0064 M final c, 10.67 eq). The monomer solution was filtered (0.2 µm PTFE syringe filter) into the second flask, and the light blue solution obtained degassed for a further 20 min. Separately, ascorbic acid (8.5 mg in 10 mL, 0.0048 M) was added to mQ:MeOH=1:2 and degassed for 20 min. Gold sensors with ω-mercaptoundecyl bromoisobutyrate SAMs were removed from the initiator solution, washed with ethanol, dried, and placed in a SCHLENK flask. The light blue reaction solution was transferred to this flask *via* cannula. A PTFE tube was pushed through the septum to enable a continuous ascorbic acid supply later-on. To initiate the polymerization, 2 mL of ascorbic acid solution (0.000 98 M final c, 1.63 eq) was added. The reaction was then shaken (50 rpm), and an additional 1 µL/ min ascorbic acid solution was continuously supplied *via* syringe pump until the reaction was quenched by exposure to air. Finally, the sensors were rinsed with mQ and ethanol, and dried.

SI-ATRP in MeOH

The same procedure was used for polymerization in MeOH, but the final c varied as follows for PNIPAM-co-MBAM$_1$: NIPAM (1.0755 g, 0.95 M final c, 792 eq), MBAM (14.8 mg, 0.0096 M final c, 8 eq), CuBr$_2$ (2.7 mg, 0.0012 M final c, 1 eq), PMDETA (26.7 µL, 0.0128 M final c, 10.67 eq). An ascorbic acid solution (8.5 mg in 10 mL, 0.0048 M) in MeOH was prepared, degassed and a 1 mL aliquot (0.000 49 M final c, 0.41 eq) was used to initiate the polymerization. Again, 1 µL min^{-1} of the ascorbic acid solution was continuously supplied *via* a syringe pump.

PNIPAM-co-NBPAM

PNIPAM brushes and PNIPAM-co-NBPAM gels were prepared under the same reaction conditions. PNIPAM-co-NBPAM gels containing 0 mol% (for brushes), 1 mol%, 2 mol% and 10 mol% were prepared. Reactions were carried out using standard SCHLENK line techniques under an inert atmosphere of N$_2$. Unless stated otherwise a 10 mL reaction volume was used.
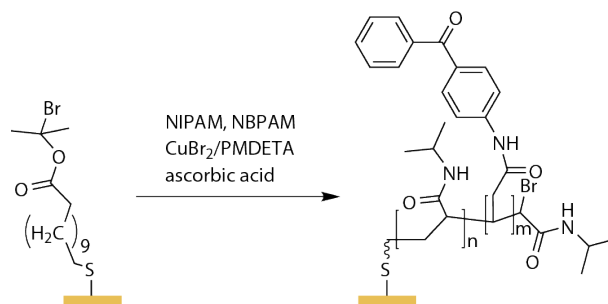
Scheme 5.2: SI-ARGET-ATRP of PNIPAM-co-NBPAM.

SI-ATRP in mQ/dioxane solvents

The reaction was performed in a similar procedure as described previously for PNIPAM-co- MBAM, but using dioxane instead of MeOH and a reaction volume of 50 mL. The reactant amounts were as follows for PNIPAM-co-NBPAM$_1$: NIPAM (2.6024 g, 0.469 M final c, 782 eq), NBPAM (0.0591 g, 0.005 M final c, 8 eq); for PNIPAM-co-NBPAM$_2$: NIPAM (2.6083 g, 0.47 M final c, 782 eq), NBPAM (0.1182 g, 0.0096 M final c, 16 eq); for PNIPAM-co-NBPAM$_{10}$: NIPAM (2.3954 g, 0.43 M final c, 720 eq), NBPAM (0.5910 g, 0.048 M final c, 80 eq); and CuBr$_2$ (0.0066 g, 0.0006 M final c, 1 eq), PMDETA (65.5 μL, 0.0064 M final c, 10.67 eq). An ascorbic acid solution (0.1725 g in 2 mL, 0.49 M) in mQ was prepared, degassed and a 1 mL aliquot (0.01 M final c, 16.7 eq) was used to initiate the polymerization.

5.4. Overview of Experiments

Table 5.2.: Overview of all experiments. * indicates a continuous ascorbic acid supply.

product	[monomer] /M	[asc. acid] /mM	[CuBr$_2$] /mM	solvent	time /h	h$_{air}$ /nm	h$_{25°C}$ /nm	h$_{35°C}$ /nm
PNIPAM	0.48	0.49*	0.6	MeOH:mQ=2:1	0.25	12	–	–
PNIPAM	0.48	0.98*	0.6	MeOH:mQ=2:1	0.5	15	100.6	33.8
PNIPAM-co-MBAM$_1$	0.48	0.98*	0.6	MeOH:mQ=2:1	0.25	18	69.4	21.5
PNIPAM-co-MBAM$_1$	0.48	0.98*	0.6	MeOH:mQ=2:1	0.5	52	289.3	71.6
PNIPAM-co-MBAM$_1$	0.48	0.98*	0.6	MeOH:mQ=2:1	0.5	11.3	40.0	19.5
PNIPAM-co-MBAM$_1$	0.48	0.98*	0.6	MeOH:mQ=2:1	0.5	–	94.2	38.4
PNIPAM-co-MBAM$_{1.12}$	0.48	0.98*	0.6	MeOH:mQ=2:1	0.5	42	104	58
PNIPAM-co-MBAM$_1$	0.48	0.98*	0.6	MeOH:mQ=2:1	1	36.3	–	–
PNIPAM-co-MBAM$_1$	0.48	0.9*	1.0	MeOH:mQ=2:1	1	37	105.4	56.7
PNIPAM-co-MBAM$_1$	0.48	0.9*	1.0	MeOH:mQ=2:1	3	49	–	–
PNIPAM-co-MBAM$_1$	0.48	0.98*	0.6	MeOH:mQ=2:1	3	41	154	69.2
PNIPAM-co-MBAM$_1$	0.48	0.98*	0.6	MeOH:mQ=2:1	1.5	47	197.4	70.9
PNIPAM-co-MBAM$_{1.08}$	0.48	0.98*	0.6	MeOH:mQ=2:1	24	48	197.4	70.9
PNIPAM	0.96	0.49*	1.2	MeOH	0.5	3.3	37.7	11.5
PNIPAM	0.48	0.98*	1.2	MeOH	4	8	–	–
PNIPAM	0.96	0.49*	1.2	MeOH	24	8	118.6	36.3
PNIPAM	0.96	0.49*	1.2	MeOH	24	14	88.2	37.4
PNIPAM-co-MBAM$_{0.55}$	0.96	0.49*	1.2	MeOH	24	30.5	115.5	30.7
PNIPAM-co-MBAM$_1$	0.96	0.49*	1.2	MeOH	1	28.7	91.8	46.9
PNIPAM-co-MBAM$_1$	0.96	0.49*	1.2	MeOH	2	28	–	–
PNIPAM-co-MBAM$_1$	0.96	0.49*	1.2	MeOH	4	28	–	–
PNIPAM-co-MBAM$_{1.32}$	0.48	0.49*	0.6	MeOH	4	13	27	19.5
PNIPAM-co-MBAM$_1$	0.96	0.49*	1.2	MeOH	12	28	–	–
PNIPAM-co-MBAM$_1$	0.96	0.49*	1.2	MeOH	12+2.5	30	–	–
PNIPAM-co-MBAM$_1$	0.96	0.49*	1.2	MeOH	24	26	72.9	38.4
PNIPAM-co-MBAM$_1$	0.96	0.49*	1.2	MeOH	24	27	62.0	41.7
PNIPAM-co-MBAM$_1$	0.96	0.49*	1.2	MeOH	30	31	83.8	43.7
PNIPAM-co-MBAM$_1$	0.96	0.49*	1.2	MeOH	48	44	108	62.8
PNIPAM-co-MBAM$_{1.07}$	0.96	0.49*	1.2	MeOH	65	32	74.5	42.2
PNIPAM-co-MBAM$_2$	0.96	0.49*	1.2	MeOH	24	26	72.1	37.8
PNIPAM-co-MBAM$_3$	0.96	0.49*	1.2	MeOH	24	31	42.4	27.2
PNIPAM-co-MBAM$_{3.71}$	0.96	0.49*	1.2	MeOH	24	22.5	58.7	39.8
PNIPAM-co-MBAM$_4$	0.96	0.49*	1.2	MeOH	24	17	73.3	38.8
PNIPAM-co-MBAM$_5$	0.96	0.49*	1.2	MeOH	24	20	47.6	38.2
PNIPAM-co-MBAM$_{10}$	0.96	0.49*	1.2	MeOH	24	8	17.4	14.2
PNIPAM-co-MBAM$_{10}$	0.96	0.49*	1.2	MeOH	24	7.7	13.5	11.6
PNIPAM	0.48	10	0.6	dioxane:mQ=1:1	0.5	44	–	–
PNIPAM-co-NBPAM$_1$	0.48	10	0.6	dioxane:mQ=1:1	0.5	–	–	–
PNIPAM-co-NBPAM$_2$	0.48	10	0.6	dioxane:mQ=1:1	0.5	31	–	–
PNIPAM-co-NBPAM$_2$	0.48	10	0.6	dioxane:mQ=1:1	0.5	23	16.2	18.7
PNIPAM-co-NBPAM$_{10}$	0.48	10	0.6	dioxane:mQ=4:1	0.5	15	–	–
PNIPAM	0.48	0.24	0.6	DMSO	4	2	–	–
PNIPAM-co-MBAM$_1$	0.48	0.24	0.6	MeOH	4	3.3	–	–
PNIPAM-co-MBAM$_1$	0.48	0.24	0.6	DMSO	4	5.5	–	–

Bibliography

[1] Simona Argentiere, Giuseppe Gigli, Mariangela Mortato Irini Gerges, and Laura Blasi. Smart microfluidics: The role of stimuli-responsive polymers in microfluidic devices. In *Advances in Microfluidics*. IntechOpen, 2012.

[2] Martien A Cohen Stuart, Wilhelm TS Huck, Jan Genzer, Marcus Müller, Christopher Ober, Manfred Stamm, Gleb B Sukhorukov, Igal Szleifer, Vladimir V Tsukruk, Marek Urban, et al. Emerging applications of stimuli-responsive polymer materials. *Nature materials*, 9(2):101–113, 2010.

[3] Tao Chen, Robert Ferris, Jianming Zhang, Robert Ducker, and Stefan Zauscher. Stimulus-responsive polymer brushes on surfaces: Transduction mechanisms and applications. *Progress in Polymer Science*, 35(1-2):94–112, 2010.

[4] Mark A Ward and Theoni K Georgiou. Thermoresponsive polymers for biomedical applications. *Polymers*, 3(3):1215–1242, 2011.

[5] Jose Ramos, Ainara Imaz, and Jacqueline Forcada. Temperature-sensitive nanogels: poly (n-vinylcaprolactam) versus poly (n-isopropylacrylamide). *Polymer Chemistry*, 3(4):852–856, 2012.

[6] Dongxiang Li, Qiang He, Yue Cui, Kewei Wang, Xiaoming Zhang, and Junbai Li. Thermosensitive copolymer networks modify gold nanoparticles for nanocomposite entrapment. *Chemistry–A European Journal*, 13(8):2224–2229, 2007.

[7] Xiaomei Ma, Yanjun Cui, Xian Zhao, Sixun Zheng, and Xiaozhen Tang. Different deswelling behavior of temperature-sensitive microgels of poly (n-isopropylacrylamide) crosslinked by polyethyleneglycol dimethacrylates. *Journal of colloid and interface science*, 276(1):53–59, 2004.

[8] José Ribeiro, Francisco Mota, Tarique Cavalcante, Ingrid Nogueira, Victor Gondim, Victor Albuquerque, and Auzuir Alexandria. Analysis of man-machine interfaces in upper-limb prosthesis: A review. *Robotics*, 8(1):16, 2019.

[9] Yichen Hu, Longchao Da, Weiming Zhang, Chenyang Yang, Yang Wu, and Guirong Dong. Tissue organ analogue manufacturing by 3d bio-printing technology for tissue engineering applications. In *Proceedings of the Seventh Asia International Symposium on Mechatronics*, pages 911–916. Springer, 2020.

[10] A Fatih Sarioglu, Nicola Aceto, Nikola Kojic, Maria C Donaldson, Mahnaz Zeinali, Bashar Hamza, Amanda Engstrom, Huili Zhu, Tilak K Sundaresan, David T Miyamoto, et al. A microfluidic device for label-free, physical capture of circulating tumor cell clusters. *Nature methods*, 12(7):685, 2015.

[11] Wentao Su, Hongjing Li, Wenwen Chen, and Jianhua Qin. Microfluidic strategies for label-free exosomes isolation and analysis. *TrAC Trends in Analytical Chemistry*, 2019.

[12] Matthew A Cooper. Label-free screening of bio-molecular interactions. *Analytical and bioanalytical chemistry*, 377(5):834–842, 2003.

[13] Paul J Flory. The configuration of real polymer chains. *The Journal of Chemical Physics*, 17(3):303–310, 1949.

[14] Guohua Chen and Allan S Hoffman. Graft copolymers that exhibit temperature-induced phase transitions over a wide range of ph. *Nature*, 373(6509):49–52, 1995.

[15] Allan S Hoffman. "intelligent" polymers in medicine and biotechnology. *Artificial organs*, 19(5):458–467, 1995.

[16] Krzysztof Matyjaszewski, Peter J Miller, Nisha Shukla, Boonchuan Immaraporn, Andrew Gelman, Barry B Luokala, Tiberiu M Siclovan, Guido Kickelbick, Thomas Vallant, Helmuth Hoffmann, et al. Polymers at interfaces: using atom transfer radical polymerization in the controlled growth of homopolymers and block copolymers from silicon surfaces in the absence of untethered sacrificial initiator. *Macromolecules*, 32(26):8716–8724, 1999.

[17] Robert B Grubbs. Nitroxide-mediated radical polymerization: limitations and versatility. *Polymer Reviews*, 51(2):104–137, 2011.

[18] Susanne Hansson, Emma Ostmark, Anna Carlmark, and Eva Malmstrom. Arget atrp for versatile grafting of cellulose using various monomers. *ACS applied materials & interfaces*, 1(11):2651–2659, 2009.

[19] Markus Müllner and Axel HE Müller. Cylindrical polymer brushes–anisotropic building blocks, unimolecular templates and particulate nanocarriers. *Polymer*, 98:389–401, 2016.

[20] Gustav Emilsson, Kunli Xiong, Yusuke Sakiyama, Bita Malekian, Viktor Ahlberg Gagnér, Rafael L Schoch, Roderick YH Lim, and Andreas B Dahlin. Polymer brushes in solid-state nanopores form an impenetrable entropic barrier for proteins. *Nanoscale*, 10(10):4663–4669, 2018.

[21] Dale L Huber, Ronald P Manginell, Michael A Samara, Byung-Il Kim, and Bruce C Bunker. Programmed adsorption and release of proteins in a microfluidic device. *Science*, 301(5631):352–354, 2003.

[22] Anna Bratek-Skicki, Vanina Cristaudo, Jerome Savocco, Sylvain Nootens, Pierre Morsomme, Arnaud Delcorte, and Christine Dupont-Gillain. Mixed polymer brushes for the selective capture and release of proteins. *Biomacromolecules*, 20(2):778–789, 2019.

[23] Yan Xu, Misato Shinomiya, and Atsushi Harada. Soft matter-regulated active nanovalves locally self-assembled in femtoliter nanofluidic channels. *Advanced Materials*, 28(11):2209–2216, 2016.

[24] Bin Zhao and William J Brittain. Polymer brushes: surface-immobilized macromolecules. *Progress in Polymer Science*, 25(5):677–710, 2000.

[25] Shikha Somani, Eric SG Shaqfeh, and J Ravi Prakash. Effect of solvent quality on the coil- stretch transition. *Macromolecules*, 43(24):10679–10691, 2010.

[26] Jan W. Gooch. *Theta Solvent*, pages 747–747. Springer New York, New York, NY, 2011.

[27] Gerard Fleer, MA Cohen Stuart, Jan MHM Scheutjens, T Cosgrove, and B Vincent. *Polymers at interfaces*. Springer Science & Business Media, 1993.

[28] William J Brittain and Sergiy Minko. A structural definition of polymer brushes. *Journal of Polymer Science Part A: Polymer Chemistry*, 45(16):3505–3512, 2007.

[29] Jürgen Rühe. *Polymer Brushes: On the Way to Tailor-Made Surfaces*, pages 1–31. John Wiley & Sons, Ltd, 2005.

[30] EB Zhulina, OV Borisov, Victor A Pryamitsyn, and TM Birshtein. Coil-globule type transitions in polymers. 1. collapse of layers of grafted polymer chains. *Macromolecules*, 24(1):140–149, 1991.

[31] PG De Gennes. Scaling theory of polymer adsorption. *Journal de physique*, 37(12):1445–1452, 1976.

[32] S Alexander. Adsorption of chain molecules with a polar head a scaling description. *Journal De Physique*, 38(8):983–987, 1977.

[33] Rudy Van Der Haegen and Bernard W Ready. Phase separation and pulse-induced critical scattering. *Pergamon Press plc, Comprehensive Polymer Science: the Synthesis, Characterization, Reactions & Applications of Polymers.*, 2:121–134, 1989.

[34] Paul J Flory. *Principles of polymer chemistry.* Cornell University Press, 1953.

[35] Omar Yassine, EQ Li, Ahmed Alfadhel, A Zaher, Mincho Kavaldzhiev, Sigurdur T Thoroddsen, and Jürgen Kosel. Magnetically triggered monodispersed nanocomposite fabricated by microfluidic approach for drug delivery. *International Journal of Polymer Science*, 2016, 2016.

[36] Cong Yu, Senol Mutlu, Ponnambalam Selvaganapathy, Carlos H Mastrangelo, Frantisek Svec, and Jean MJ Fréchet. Flow control valves for analytical microfluidic chips without mechanical parts based on thermally responsive monolithic polymers. *Analytical Chemistry*, 75(8):1958–1961, 2003.

[37] Jesse C Kelly, Nicholas L Degrood, and Mark E Roberts. Li-ion battery shut-off at high temperature caused by polymer phase separation in responsive electrolytes. *Chemical Communications*, 51(25):5448–5451, 2015.

[38] Jan Seuring and Seema Agarwal. Polymers with upper critical solution temperature in aqueous solution. *Macromolecular rapid communications*, 33(22):1898–1920, 2012.

[39] Jan Seuring and Seema Agarwal. Polymers with upper critical solution temperature in aqueous solution: unexpected properties from known building blocks, 2013.

[40] Qi Zhong, Ezzeldin Metwalli, Gunar Kaune, Monika Rawolle, Achille M Bivigou-Koumba, André Laschewsky, Christine M Papadakis, Robert Cubitt, and Peter Müller-Buschbaum. Switching kinetics of thin thermo-responsive hydrogel films of poly (monomethoxy-diethyleneglycol-acrylate) probed with in situ neutron reflectivity. *Soft Matter*, 8(19):5241–5249, 2012.

[41] Sabrina Hocine and Min-Hui Li. Thermoresponsive self-assembled polymer colloids in water. *Soft Matter*, 9(25):5839–5861, 2013.

[42] Martina Keerl and Walter Richtering. Synergistic depression of volume phase transition temperature in copolymer microgels. *Colloid and Polymer Science*, 285(4):471–474, 2007.

[43] Jochen Kleinen and Walter Richtering. Rearrangements in and release from responsive microgel- polyelectrolyte complexes induced by temperature and time. *The Journal of Physical Chemistry B*, 115(14):3804–3810, 2011.

[44] He Cheng, Lei Shen, and Chi Wu. Lls and ftir studies on the hysteresis in association and dissociation of poly (n-isopropylacrylamide) chains in water. *Macromolecules*, 39(6):2325–2329, 2006.

[45] Seung Geol Lee, Tod A Pascal, Wonsang Koh, Giuseppe F Brunello, William A Goddard III, and Seung Soon Jang. Deswelling mechanisms of surface-grafted poly (nipaam) brush: molecular dynamics simulation approach. *The Journal of Physical Chemistry C*, 116(30):15974–15985, 2012.

[46] L Andrew Lyon, Zhiyong Meng, Neetu Singh, Courtney D Sorrell, and Ashlee St John. Thermoresponsive microgel-based materials. *Chemical Society Reviews*, 38(4):865–874, 2009.

[47] Thorsten Tönsing and Christian Oldiges. Molecular dynamic simulation study on structure of water in crosslinked poly (n-isopropylacrylamide) hydrogels. *Physical Chemistry Chemical Physics*, 3(24):5542–5549, 2001.

[48] Rejane Andrade Batista, Caio Gomide Otoni, and Paula J.P. Espitia. Chapter 3 - fundamentals of chitosan-based hydrogels: elaboration and characterization techniques. In Alina-Maria Holban and Alexandru Mihai Grumezescu, editors, *Materials for Biomedical Engineering*, pages 61 – 81. Elsevier, 2019.

[49] Martien A Cohen Stuart, Wilhelm TS Huck, Jan Genzer, Marcus Müller, Christopher Ober, Manfred Stamm, Gleb B Sukhorukov, Igal Szleifer, Vladimir V Tsukruk, Marek Urban, et al. Emerging applications of stimuli-responsive polymer materials. *Nature materials*, 9(2):101–113, 2010.

[50] Ryan Toomey, Daniel Freidank, and Jürgen Rühe. Swelling behavior of thin, surface-attached polymer networks. *Macromolecules*, 37(3):882–887, 2004.

[51] Ang Li, Edmondo M Benetti, Davide Tranchida, Jarred N Clasohm, Holger Schoenherr, and Nicholas D Spencer. Surface-grafted, covalently cross-linked hydrogel brushes with tunable interfacial and bulk properties. *Macromolecules*, 44(13):5344–5351, 2011.

[52] Ella S Dehghani, Shivaprakash N Ramakrishna, Nicholas D Spencer, and Edmondo M Benetti. Controlled crosslinking is a tool to precisely modulate the

nanomechanical and nanotribological properties of polymer brushes. *Macromolecules*, 50(7):2932–2941, 2017.

[53] Robert Pelton. Temperature-sensitive aqueous microgels. *Advances in colloid and interface science*, 85(1):1–33, 2000.

[54] Clinton D Jones and L Andrew Lyon. Shell-restricted swelling and core compression in poly (n-isopropylacrylamide) core- shell microgels. *Macromolecules*, 36(6):1988–1993, 2003.

[55] Pik Yin Lai and Avi Halperin. Polymer brush at high coverage. *Macromolecules*, 24(17):4981–4982, 1991.

[56] Manjesh K Singh, Patrick Ilg, Rosa M Espinosa-Marzal, Martin Kröger, and Nicholas D Spencer. Effect of crosslinking on the microtribological behavior of model polymer brushes. *Tribology Letters*, 63(2):17, 2016.

[57] Markus Stieger, Walter Richtering, Jan Skov Pedersen, and Peter Lindner. Small-angle neutron scattering study of structural changes in temperature sensitive microgel colloids. *The Journal of chemical physics*, 120(13):6197–6206, 2004.

[58] Jinghui Zhang, Zhiwei Huang, and Dan Liu. Efficient protein-repelling thin films regulated by chain mobility of low-tg polymers with increased stability via crosslinking. *Applied Surface Science*, 426:796–803, 2017.

[59] Qiang Wei, Tobias Becherer, Paul-Ludwig Michael Noeske, Ingo Grunwald, and Rainer Haag. A universal approach to crosslinked hierarchical polymer multilayers as stable and highly effective antifouling coatings. *Advanced Materials*, 26(17):2688–2693, 2014.

[60] Yunhua Chen, Nicholas Ballard, and Stefan AF Bon. Waterborne polymer nanogels non-covalently crosslinked by multiple hydrogen bond arrays. *Polymer Chemistry*, 4(2):387–392, 2013.

[61] Wenxi Huang, Gregory L Baker, and Merlin L Bruening. Controlled synthesis of cross-linked ultrathin polymer films by using surface-initiated atom transfer radical polymerization. *Angewandte Chemie International Edition*, 40(8):1510–1512, 2001.

[62] Inga Lilge and Holger Schönherr. Covalently cross-linked poly (acrylamide) brushes on gold with tunable mechanical properties via surface-initiated atom transfer radical polymerization. *European polymer journal*, 49(8):1943–1951, 2013.

[63] Tobias Widmann, Lucas P Kreuzer, Nuri Hohn, Lorenz Bießmann, Kun Wang, Stephan Rinner, Jean-Francois Moulin, Andreas J Schmid, Yvonne Hannappel, Oliver Wrede, et al. Hydration and solvent exchange induced swelling and deswelling of homogeneous poly (n-isopropylacrylamide) microgel thin films. *Langmuir*, 35(49):16341–16352, 2019.

[64] Stephan Harms, Klaus Raetzke, Franz Faupel, Werner Egger, L Ravello, André Laschewsky, Weinan Wang, and Peter Müller-Buschbaum. Free volume and swelling in thin films of poly (n-isopropylacrylamide) end-capped with n-butyltrithiocarbonate. *Macromolecular rapid communications*, 31(15):1364–1367, 2010.

[65] Rafael Contreras-Caceres, Leonard Schellkopf, Cristina Fernandez-Lopez, Isabel Pastoriza-Santos, Jorge Perez-Juste, and Manfred Stamm. Effect of the cross-linking density on the thermoresponsive behavior of hollow pnipam microgels. *Langmuir*, 31(3):1142–1149, 2015.

[66] Colin D Bain, E Barry Troughton, Yu Tai Tao, Joseph Evall, George M Whitesides, and Ralph G Nuzzo. Formation of monolayer films by the spontaneous assembly of organic thiols from solution onto gold. *Journal of the American Chemical Society*, 111(1):321–335, 1989.

[67] Mengxing Li, Bruno Bresson, F Cousin, Christian Fretigny, and Yvette Tran. Sub-micrometric films of surface-attached polymer network with temperature-responsive properties. *Langmuir*, 31(42):11516–11524, 2015.

[68] Lucila Navarro, Loryn E Theune, and Marcelo Calderón. Effect of crosslinking density on thermoresponsive nanogels: A study on the size control and the kinetics release of biomacromolecules. *European Polymer Journal*, page 109478, 2020.

[69] Daniel Finley, Xiang Chen, and Kylie J Walters. Gates, channels, and switches: elements of the proteasome machine. *Trends in biochemical sciences*, 41(1):77–93, 2016.

[70] James Gumbart and Klaus Schulten. Structural determinants of lateral gate opening in the protein translocon. *Biochemistry*, 46(39):11147–11157, 2007.

[71] Caterina Strambio-De-Castillia, Mario Niepel, and Michael P Rout. The nuclear pore complex: bridging nuclear transport and gene regulation. *Nature reviews Molecular cell biology*, 11(7):490–501, 2010.

[72] Takuya Shiota, Kenichiro Imai, Jian Qiu, Victoria L Hewitt, Khershing Tan, Hsin-Hui Shen, Noriyuki Sakiyama, Yoshinori Fukasawa, Sikander Hayat, Megumi Kamiya, et al. Molecular architecture of the active mitochondrial protein gate. *Science*, 349(6255):1544–1548, 2015.

[73] Felix Kessler and Danny J Schnell. A gtpase gate for protein import into chloroplasts. *Nature structural biology*, 9(2):81, 2002.

[74] Laura I Davis. The nuclear pore complex. *Annual review of biochemistry*, 64(1):865–896, 1995.

[75] HG Callan, JT Randall, and SG Tomlin. An electron microscope study of the nuclear membrane. *Nature*, 163(4138):280–280, 1949.

[76] Terence D Allen, JM Cronshaw, Steven Bagley, Elena Kiseleva, and Martin W Goldberg. The nuclear pore complex: mediator of translocation between nucleus and cytoplasm. *Journal of cell science*, 113(10):1651–1659, 2000.

[77] Janet M Cronshaw, Andrew N Krutchinsky, Wenzhu Zhang, Brian T Chait, and Michael J Matunis. Proteomic analysis of the mammalian nuclear pore complex. *The Journal of cell biology*, 158(5):915–927, 2002.

[78] Tijana Jovanovic-Talisman, Jaclyn Tetenbaum-Novatt, Anna Sophia McKenney, Anton Zilman, Reiner Peters, Michael P Rout, and Brian T Chait. Artificial nanopores that mimic the transport selectivity of the nuclear pore complex. *Nature*, 457(7232):1023–1027, 2009.

[79] Frank Alber, Svetlana Dokudovskaya, Liesbeth M Veenhoff, Wenzhu Zhang, Julia Kipper, Damien Devos, Adisetyantari Suprapto, Orit Karni-Schmidt, Rosemary Williams, Brian T Chait, et al. The molecular architecture of the nuclear pore complex. *Nature*, 450(7170):695–701, 2007.

[80] Daniel H Lin, Tobias Stuwe, Sandra Schilbach, Emily J Rundlet, Thibaud Perriches, George Mobbs, Yanbin Fan, Karsten Thierbach, Ferdinand M Huber, Leslie N Collins, et al. Architecture of the nuclear pore complex symmetric core. *Science (New York, NY)*, 352(6283):aaf1015, 2016.

[81] Stefan W Kowalczyk, Larisa Kapinos, Timothy R Blosser, Tomás Magalhães, Pauline Van Nies, Roderick YH Lim, and Cees Dekker. Single-molecule transport across an individual biomimetic nuclear pore complex. *Nature nanotechnology*, 6(7):433, 2011.

[82] Reiner Peters. Functionalization of a nanopore: the nuclear pore complex paradigm. *Biochimica et Biophysica Acta (BBA)-Molecular Cell Research*, 1793(10):1533–1539, 2009.

[83] Mathilde Lepoitevin, Tianji Ma, Mikhael Bechelany, Jean-Marc Janot, and Sebastien Balme. Functionalization of single solid state nanopores to mimic biological ion channels: A review. *Advances in colloid and interface science*, 250:195–213, 2017.

[84] Zifan Tang, Daihua Zhang, Weiwei Cui, Hao Zhang, Wei Pang, and Xuexin Duan. Fabrications, applications and challenges of nanopores: a mini review. *Nanomaterials and Nanotechnology*, 6:35, 2016.

[85] Rob D Coalson, Afshin Eskandari Nasrabad, David Jasnow, and Anton Zilman. A polymer-brush-based nanovalve controlled by nanoparticle additives: design principles. *The Journal of Physical Chemistry B*, 119(35):11858–11866, 2015.

[86] Zhuang Liu, Wei Wang, Rui Xie, Xiao-Jie Ju, and Liang-Yin Chu. Stimuli-responsive smart gating membranes. *Chemical Society Reviews*, 45(3):460–475, 2016.

[87] Daniel Branton, David W Deamer, Andre Marziali, Hagan Bayley, Steven A Benner, Thomas Butler, Massimiliano Di Ventra, Slaven Garaj, Andrew Hibbs, Xiaohua Huang, et al. The potential and challenges of nanopore sequencing. In *Nanoscience and technology: A collection of reviews from Nature Journals*, pages 261–268. World Scientific, 2010.

[88] Bala Murali Venkatesan and Rashid Bashir. Nanopore sensors for nucleic acid analysis. *Nature nanotechnology*, 6(10):615, 2011.

[89] Gustav Emilsson, Yusuke Sakiyama, Bita Malekian, Kunli Xiong, Zeynep Adali-Kaya, Roderick YH Lim, and Andreas B Dahlin. Gating protein transport in solid state nanopores by single molecule recognition. *ACS central science*, 4(8):1007–1014, 2018.

[90] Liang-Yin Chu, Takuya Niitsuma, Takeo Yamaguchi, and Shin-ichi Nakao. Thermoresponsive transport through porous membranes with grafted pnipam gates. *AIChE Journal*, 49(4):896–909, 2003.

[91] Halima Alem, Anne-Sophie Duwez, Perrine Lussis, Pascale Lipnik, Alain M Jonas, and Sophie Demoustier-Champagne. Microstructure and thermo-responsive behav-

ior of poly (n-isopropylacrylamide) brushes grafted in nanopores of track-etched membranes. *Journal of Membrane Science*, 308(1-2):75–86, 2008.

[92] Sergiy Minko. Grafting on solid surfaces:"grafting to" and "grafting from" methods. In *Polymer surfaces and interfaces*, pages 215–234. Springer, 2008.

[93] Marion K Brinks and Armido Studer. Polymer brushes by nitroxide-mediated polymerization. *Macromolecular rapid communications*, 30(13):1043–1057, 2009.

[94] John Chiefari, YK Chong, Frances Ercole, Julia Krstina, Justine Jeffery, Tam PT Le, Roshan TA Mayadunne, Gordon F Meijs, Catherine L Moad, Graeme Moad, et al. Living free-radical polymerization by reversible addition- fragmentation chain transfer: the raft process. *Macromolecules*, 31(16):5559–5562, 1998.

[95] Krzysztof Matyjaszewski. Atom transfer radical polymerization (atrp): current status and future perspectives. *Macromolecules*, 45(10):4015–4039, 2012.

[96] Jin-Shan Wang and Krzysztof Matyjaszewski. Controlled/" living" radical polymerization. atom transfer radical polymerization in the presence of transition-metal complexes. *Journal of the American Chemical Society*, 117(20):5614–5615, 1995.

[97] Mitsuru Kato, Masami Kamigaito, Mitsuo Sawamoto, and Toshinobu Higashimura. Polymerization of methyl methacrylate with the carbon tetrachloride/dichlorotris-(triphenylphosphine) ruthenium (ii)/methylaluminum bis (2, 6-di-tert-butylphenoxide) initiating system: possibility of living radical polymerization. *Macromolecules*, 28(16):1721–1723, 1995.

[98] Guido Kickelbick, Ulrich Reinöhl, Teja S Ertel, Helmut Bertagnolli, and Krzysztof Matyjaszewski. The copper catalyst in atom transfer radical polymerizations: structural observations. In *Controlled/Living Radical Polymerization*. ACS Publications, 1999.

[99] Ke Min, Haifeng Gao, and Krzysztof Matyjaszewski. Preparation of homopolymers and block copolymers in miniemulsion by atrp using activators generated by electron transfer (aget). *Journal of the American Chemical Society*, 127(11):3825–3830, 2005.

[100] Ke Min, Haifeng Gao, and Krzysztof Matyjaszewski. Use of ascorbic acid as reducing agent for synthesis of well-defined polymers by arget atrp. *Macromolecules*, 40(6):1789–1791, 2007.

[101] Wojciech Jakubowski, Ke Min, and Krzysztof Matyjaszewski. Activators regenerated by electron transfer for atom transfer radical polymerization of styrene. *Macromolecules*, 39(1):39–45, 2006.

[102] Li Niu, Shubo Deng, Gang Yu, and Jun Huang. Efficient removal of cu (ii), pb (ii), cr (vi) and as (v) from aqueous solution using an aminated resin prepared by surface-initiated atom transfer radical polymerization. *Chemical Engineering Journal*, 165(3):751–757, 2010.

[103] Ke Min, Haifeng Gao, and Krzysztof Matyjaszewski. Use of ascorbic acid as reducing agent for synthesis of well-defined polymers by arget atrp. *Macromolecules*, 40(6):1789–1791, 2007.

[104] Antonina Simakova, Saadyah E Averick, Dominik Konkolewicz, and Krzysztof Matyjaszewski. Aqueous arget atrp. *Macromolecules*, 45(16):6371–6379, 2012.

[105] Krzysztof Matyjaszewski, Hongchen Dong, Wojciech Jakubowski, Joanna Pietrasik, and Andy Kusumo. Grafting from surfaces for "everyone": Arget atrp in the presence of air. *Langmuir*, 23(8):4528–4531, 2007.

[106] Lin Yuan, Qian Yu, Dan Li, and Hong Chen. Surface modification to control protein/surface interactions. *Macromolecular bioscience*, 11(8):1031–1040, 2011.

[107] Ai T Nguyen, Jacob Baggerman, Jos MJ Paulusse, Cees JM van Rijn, and Han Zuilhof. Stable protein-repellent zwitterionic polymer brushes grafted from silicon nitride. *Langmuir*, 27(6):2587–2594, 2011.

[108] Markus Horn and Krzysztof Matyjaszewski. Solvent effects on the activation rate constant in atom transfer radical polymerization. *Macromolecules*, 46(9):3350–3357, 2013.

[109] Florian Seeliger and Krzysztof Matyjaszewski. Temperature effect on activation rate constants in atrp: new mechanistic insights into the activation process. *Macromolecules*, 42(16):6050–6055, 2009.

[110] Joachim Morick, Michael Buback, and Krzysztof Matyjaszewski. Effect of pressure on activation–deactivation equilibrium constants for atrp of methyl methacrylate. *Macromolecular Chemistry and Physics*, 213(21):2287–2292, 2012.

[111] Robert Williams Wood. On a remarkable case of uneven distribution of light in a diffraction grating spectrum. *Proceedings of the Physical Society of London*, 18(1):269, 1902.

[112] Stefan Alexander Maier. *Plasmonics: fundamentals and applications*. Springer Science & Business Media, 2007.

[113] Jiří Homola and Marek Piliarik. Surface plasmon resonance (spr) sensors. In *Surface plasmon resonance based sensors*, pages 45–67. Springer, 2006.

[114] GC Debney, Roy P Kerr, and Alfred Schild. Solutions of the einstein and einstein-maxwell equations. *Journal of Mathematical Physics*, 10(10):1842–1854, 1969.

[115] Andreas Otto. Excitation of nonradiative surface plasma waves in silver by the method of frustrated total reflection. *Zeitschrift für Physik A Hadrons and nuclei*, 216(4):398–410, 1968.

[116] Erwin Kretschmann and Heinz Raether. Radiative decay of non radiative surface plasmons excited by light. *Zeitschrift für Naturforschung A*, 23(12):2135–2136, 1968.

[117] Jiří Homola. Surface plasmon resonance sensors for detection of chemical and biological species. *Chemical reviews*, 108(2):462–493, 2008.

[118] A Otto and W Sohler. Modification of the total reflection modes in a dielectric film by one metal boundary. *Optics Communications*, 3(4):254–258, 1971.

[119] Heinz Raether. Surface plasmons on smooth surfaces. In *Surface plasmons on smooth and rough surfaces and on gratings*, pages 4–39. Springer, 1988.

[120] Rafael L Schoch and Roderick YH Lim. Non-interacting molecules as innate structural probes in surface plasmon resonance. *Langmuir*, 29(12):4068–4076, 2013.

[121] Yannic Brasse, Mareen B Muller, Matthias Karg, Christian Kuttner, Tobias AF Konig, and Andreas Fery. Magnetic and electric resonances in particle-to-film-coupled functional nanostructures. *ACS applied materials & interfaces*, 10(3):3133–3141, 2018.

[122] Gustav Emilsson, Rafael L Schoch, Philipp Oertle, Kunli Xiong, Roderick YH Lim, and Andreas B Dahlin. Surface plasmon resonance methodology for monitoring polymerization kinetics and morphology changes of brushes—evaluated with poly (n-isopropylacrylamide). *Applied Surface Science*, 396:384–392, 2017.

[123] Andreas B Dahlin, Mokhtar Mapar, Kunli Xiong, Francesco Mazzotta, Fredrik Höök, and Takumi Sannomiya. Plasmonic nanopores in metal-insulator-metal films. *Advanced Optical Materials*, 2(6):556–564, 2014.

[124] Andreas B Dahlin. Sensing applications based on plasmonic nanopores: The hole story. *Analyst*, 140(14):4748–4759, 2015.

[125] Bita Malekian, Kunli Xiong, Evan SH Kang, John Andersson, Gustav Emilsson, Marcus Rommel, Takumi Sannomiya, Magnus P Jonsson, and Andreas Dahlin. Optical properties of plasmonic nanopore arrays prepared by electron beam and colloidal lithography. *Nanoscale Advances*, 1(11):4282–4289, 2019.

[126] Kunli Xiong, Gustav Emilsson, and Andreas B Dahlin. Biosensing using plasmonic nanohole arrays with small, homogenous and tunable aperture diameters. *Analyst*, 141(12):3803–3810, 2016.

[127] Diethelm Johannsmann. The quartz crystal microbalance in soft matter research. *Fundamentals and modeling. Switzerland: Springer International Publishing*, 2015.

[128] Marina V Voinova, M Rodahl, M Jonson, and B Kasemo. Viscoelastic acoustic response of layered polymer films at fluid-solid interfaces: continuum mechanics approach. *Physica Scripta*, 59(5):391, 1999.

[129] Thomas J Lane. Ultrasonic rheology of mixed-phase systems: Using a qcm as an effective rheological device–theory and applications for combined surface and bulk rheology. In *Amphiphiles: Molecular Assembly and Applications*, pages 145–174. ACS Publications, 2011.

[130] T Nomura and M Okuhara. Frequency shifts of piezoelectric quartz crystals immersed in organic liquids. *Analytica Chimica Acta*, 142:281–284, 1982.

[131] Kenichi Sakai. Quartz crystal microbalance with dissipation monitoring (qcm-d). In *Measurement Techniques and Practices of Colloid and Interface Phenomena*. Springer, 2019.

[132] Fredrik Höök and Bengt Kasemo. The qcm-d technique for probing biomacromolecular recognition reactions. In *Piezoelectric sensors*, pages 425–447. Springer, 2006.

[133] Fredrik Höök, Bengt Kasemo, Tommy Nylander, Camilla Fant, Kristin Sott, and Hans Elwing. Variations in coupled water, viscoelastic properties, and film thickness of a mefp-1 protein film during adsorption and cross-linking: a quartz crystal microbalance with dissipation monitoring, ellipsometry, and surface plasmon resonance study. *Analytical chemistry*, 73(24):5796–5804, 2001.

[134] Lloyd B Eldred, William P Baker, and Anthony N Palazotto. Kelvin-voigt versus fractional derivative model as constitutive relations for viscoelastic materials. *AIAA journal*, 33(3):547–550, 1995.

[135] Ilya Reviakine, Diethelm Johannsmann, and Ralf P Richter. Hearing what you cannot see and visualizing what you hear: interpreting quartz crystal microbalance data from solvated interfaces, 2011.

[136] Leena Patra and Ryan Toomey. Viscoelastic response of photo-cross-linked poly (n-isopropylacrylamide) coatings by qcm-d. *Langmuir*, 26(7):5202–5207, 2009.

[137] Yungwan Kwak, Andrew JD Magenau, and Krzysztof Matyjaszewski. Arget atrp of methyl acrylate with inexpensive ligands and ppm concentrations of catalyst. *Macromolecules*, 44(4):811–819, 2011.

[138] Tommy Munk, Stefania Baldursdottir, Sami Hietala, Thomas Rades, Markus Nuopponen, Katriina Kalliomäki, Heikki Tenhu, Jukka Rantanen, and Clare J Strachan. Investigation of the phase separation of pnipam using infrared spectroscopy together with multivariate data analysis. *Polymer*, 54(26):6947–6953, 2013.

[139] Tennyson Smith. The hydrophilic nature of a clean gold surface. *Journal of Colloid and Interface Science*, 75(1):51–55, 1980.

[140] Patricia V Mendoca, Saadyah E Averick, Dominik Konkolewicz, Armenio C Serra, Anatoliy V Popov, Tamaz Guliashvili, Krzysztof Matyjaszewski, and Jorge FJ Coelho. Straightforward arget atrp for the synthesis of primary amine polymethacrylate with improved chain-end functionality under mild reaction conditions. *Macromolecules*, 47(14):4615–4621, 2014.

[141] Marc P Bradshaw, Celia Barril, Andrew C Clark, Paul D Prenzler, and Geoffrey R Scollary. Ascorbic acid: a review of its chemistry and reactivity in relation to a wine environment. *Critical reviews in food science and nutrition*, 51(6):479–498, 2011.

[142] Joydeb Mandal, RS Varunprasaath, Wenqing Yan, Mohammad Divandari, Nicholas D Spencer, and Matthias Dübner. In situ monitoring of si-atrp throughout multiple reinitiations under flow by means of a quartz crystal microbalance. *RSC advances*, 8(36):20048–20055, 2018.

[143] Wade A Braunecker, Nicolay V Tsarevsky, Armando Gennaro, and Krzysztof Matyjaszewski. Thermodynamic components of the atom transfer radical polymerization equilibrium: quantifying solvent effects. *Macromolecules*, 42(17):6348–6360, 2009.

[144] Wade A Braunecker and Krzysztof Matyjaszewski. Controlled/living radical polymerization: Features, developments, and perspectives. *Progress in polymer science*, 32(1):93–146, 2007.

[145] Carlos MR Abreu, Arménio C Serra, Anatoliy V Popov, Krzysztof Matyjaszewski, Tamaz Guliashvili, and Jorge FJ Coelho. Ambient temperature rapid sara atrp of acrylates and methacrylates in alcohol–water solutions mediated by a mixed sulfite/cu (ii) br 2 catalytic system. *Polymer Chemistry*, 4(23):5629–5636, 2013.

[146] Carlos MR Abreu, Patrícia V Mendonça, Arménio C Serra, Jorge FJ Coelho, Anatoliy V Popov, and Tamaz Guliashvili. Accelerated ambient-temperature atrp of methyl acrylate in alcohol–water solutions with a mixed transition-metal catalyst system. *Macromolecular Chemistry and Physics*, 213(16):1677–1687, 2012.

[147] Joana P Mendes, Patrícia V Mendonça, Pedro Maximiano, Carlos MR Abreu, Tamaz Guliashvili, Arménio C Serra, and Jorge FJ Coelho. Getting faster: low temperature copper-mediated sara atrp of methacrylates, acrylates, styrene and vinyl chloride in polar media using sulfolane/water mixtures. *RSC advances*, 6(12):9598–9603, 2016.

[148] Mariano J Garcia-Soto, Karsten Haupt, and Carlo Gonzato. Synthesis of molecularly imprinted polymers by photo-iniferter polymerization under visible light. *Polymer Chemistry*, 8(33):4830–4834, 2017.

[149] Dapeng Zhou, Xiang Gao, Wen-jun Wang, and Shiping Zhu. Termination of surface radicals and kinetic modeling of atrp grafting from flat surfaces by addition of deactivator. *Macromolecules*, 45(3):1198–1207, 2012.

[150] Yeongun Ko and Jan Genzer. Spontaneous degrafting of weak and strong polycationic brushes in aqueous buffer solutions. *Macromolecules*, 52(16):6192–6200, 2019.

[151] Esther K Riga, Julia S Saar, Roman Erath, Michelle Hechenbichler, and Karen Lienkamp. On the limits of benzophenone as cross-linker for surface-attached polymer hydrogels. *Polymers*, 9(12):686, 2017.

[152] Scott K Christensen, Maria C Chiappelli, and Ryan C Hayward. Gelation of copolymers with pendent benzophenone photo-cross-linkers. *Macromolecules*, 45(12):5237–5246, 2012.

[153] Ernö Pretsch, Philippe Bühlmann, and Martin Badertscher. *Spektroskopische Daten zur Strukturaufklärung organischer Verbindungen*. Springer-Verlag, 2010.

[154] Nityanand Sharma, Hamid Keshmiri, Xiaodong Zhou, Ten It Wong, Christian Petri, Ulrich Jonas, Bo Liedberg, and Jakub Dostalek. Tunable plasmonic nanohole ar-

rays actuated by a thermoresponsive hydrogel cushion. *The Journal of Physical Chemistry C*, 120(1):561–568, 2016.

[155] P Yeh. Optical waves in layered media, edited by be saleh wiley, 1998.

[156] Dmitry I Yakubovsky, Aleksey V Arsenin, Yury V Stebunov, Dmitry Yu Fedyanin, and Valentyn S Volkov. Optical constants and structural properties of thin gold films. *Optics express*, 25(21):25574–25587, 2017.

[157] Bita Malekian, Kunli Xiong, Gustav Emilsson, Jenny Andersson, Cecilia Fager, Eva Olsson, Elin M Larsson-Langhammer, and Andreas B Dahlin. Fabrication and characterization of plasmonic nanopores with cavities in the solid support. *Sensors*, 17(6):1444, 2017.

A. Appendix

A.1. Additional SPR Results
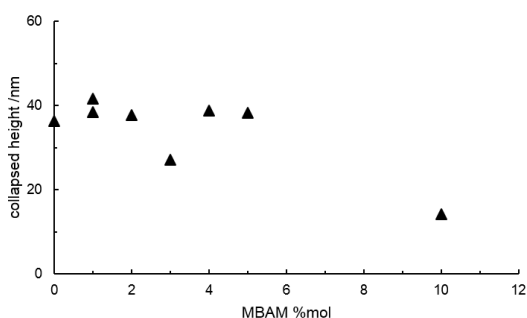
Figure A.1.: The collapsed height measured in PBS at 35 °C remains almost constant for more MBAM content in PNIPAM-co-MBAM networks.
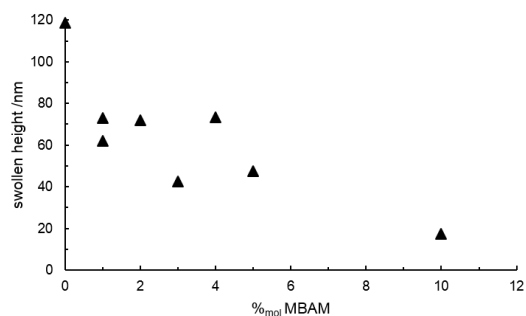
Figure A.2.: The swollen height measured in PBS at 25 °C decreases with more MBAM content in PNIPAM-co-MBAM networks.
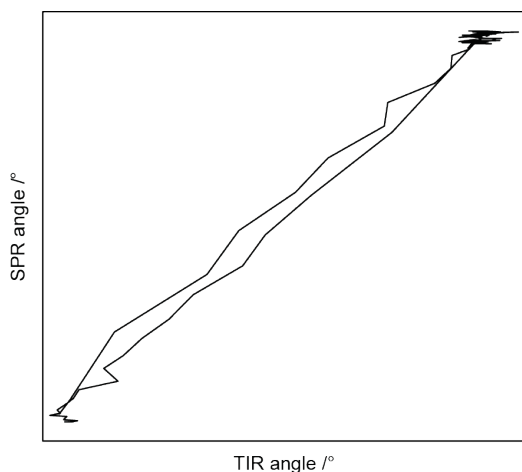

Figure A.3.: The linear relationship of TIR and SPR shifts upon 35 kDa PEG injection at 35 °C confirm no interaction between the probe and PNIPAM-co-NBPAM in the collapsed.
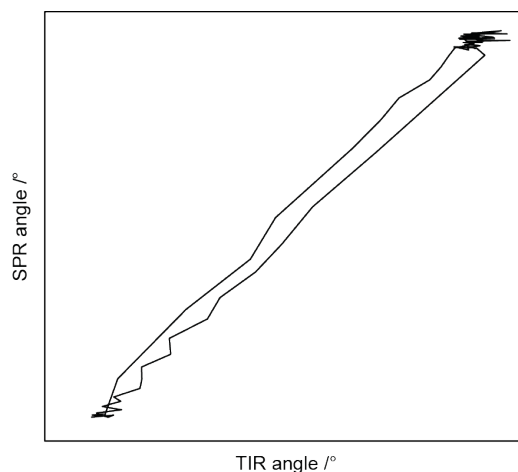
Figure A.4.: The linear relationship of TIR and SPR shifts upon 35 kDa PEG injection at 25 °C confirm no interaction between the probe and PNIPAM-co-NBPAM in the swollen state.
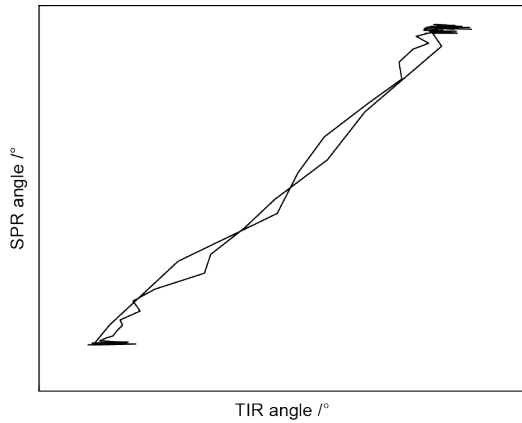
Figure A.5.: The linear relationship of TIR and SPR shifts upon 35 kDa PEG injection at 35 °C confirm no interaction between the probe and PNIPAM-co-MBAM in the collapsed.
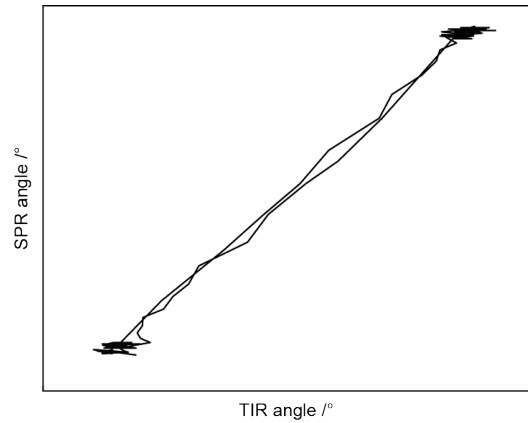
Figure A.6.: The linear relationship of TIR and SPR shifts upon 35 kDa PEG injection at 25 °C confirm no interaction between the probe and PNIPAM-co-MBAM in the swollen state.

A.1.1. Refractive Indices Obtained from SPR
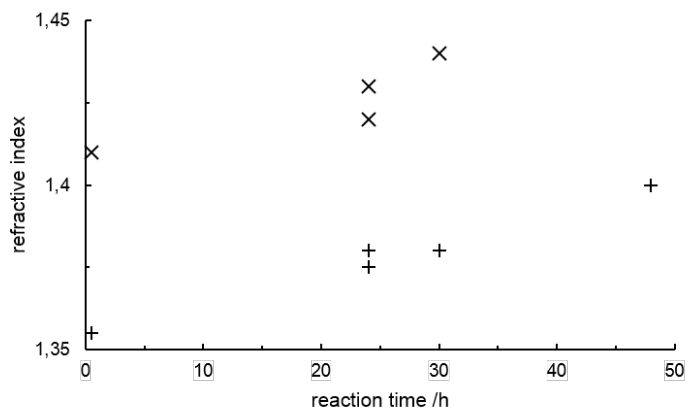
Figure A.7.: The refractive indices vs. reaction time for PNIPAM-co-MBAM$_1$ prepared in MeOH shows no trend. Crosses represent the n measured at 35 °C and plus those obtained from spectra at 25 °C.
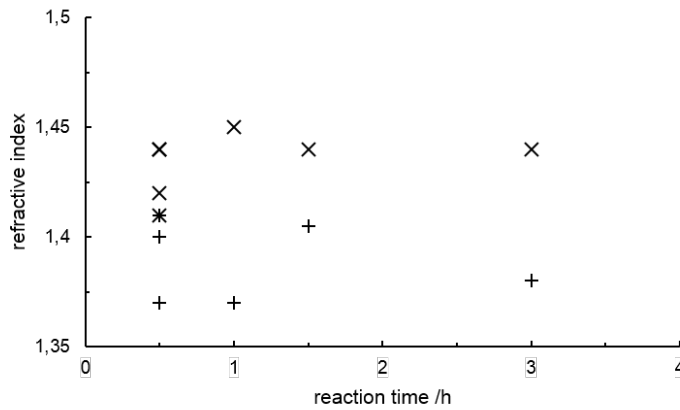
Figure A.8.: The refractive indices vs. reaction time for PNIPAM-co-MBAM$_1$ prepared in MeOH:mQ=2:1 shows no trend. Crosses represent the n measured at 35 °C and plus those obtained from spectra at 25 °C.

A.1.2. Additional Insplorion Measurements
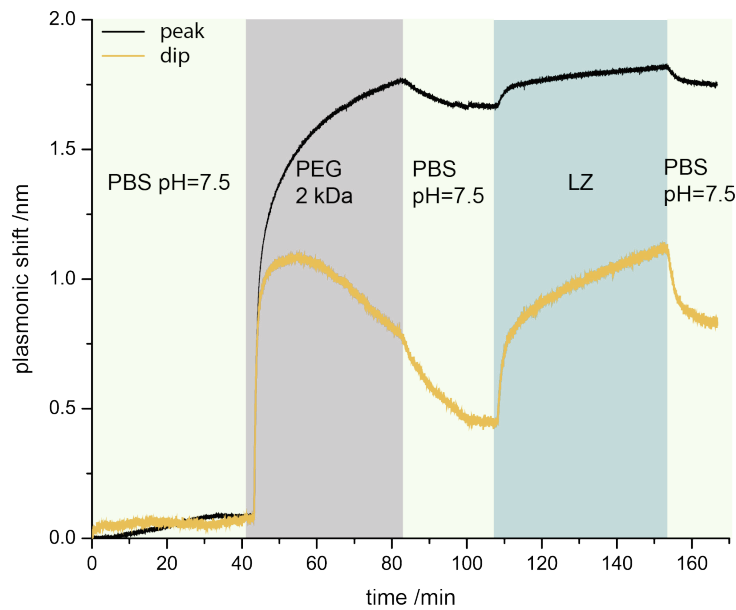
Figure A.9.: In a test experiment, 2 kDa PEG was first grafted to a nanopore containing gold sensor. After rinsing with PBS, LZ was supplied at a pH-value of 7.5, resulting in a shift of peak and dip position of +0.15 and +0.3, respectively.

A.2. Additional QCM-D Plots
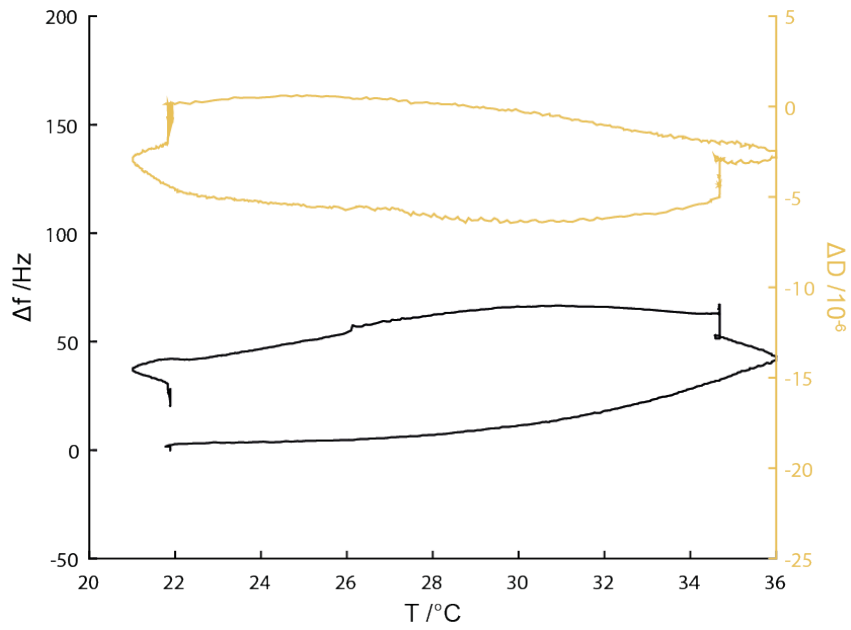
Figure A.10.: QCM-D plot of PNIPAM-co-MBAM$_4$ prepared in MeOH in 24 h.
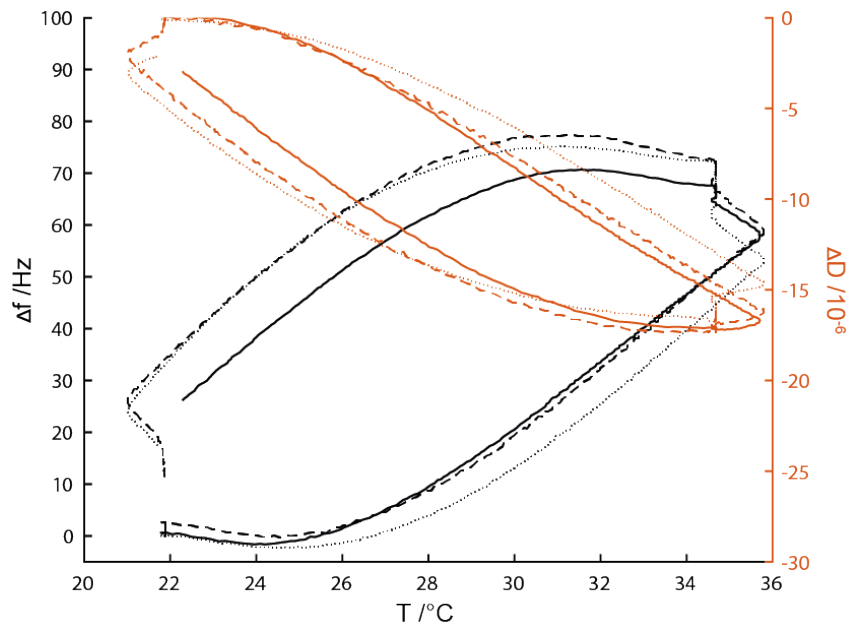

Figure A.11.: QCM-D plot for bare gold sensors mounted in all three used flow cells to reveal potential errors originating from temperature, flow or sensing inaccuracies.
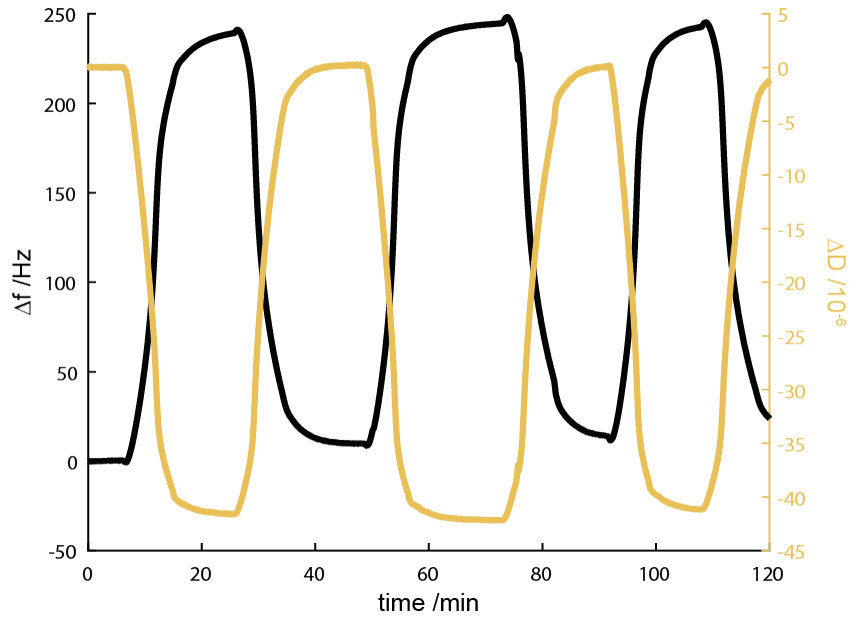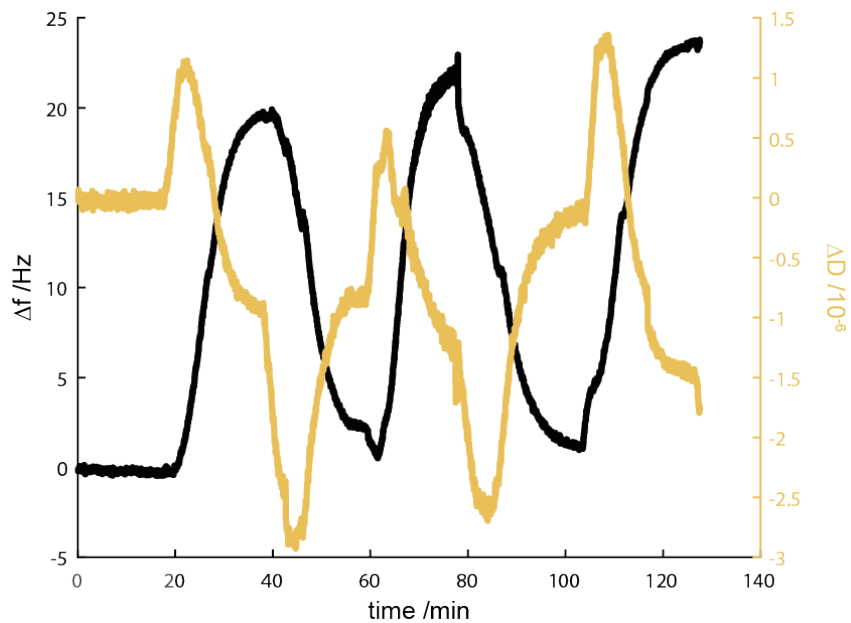
Figure A.12.: QCM-D plot of a swelling experiment for PNIPAM brushes in PBS (pH=7.5). Three temperature increases from $22\,°C$ to $35\,°C$ reveal the reversible swell and collapse behaviour of the polymer layer.
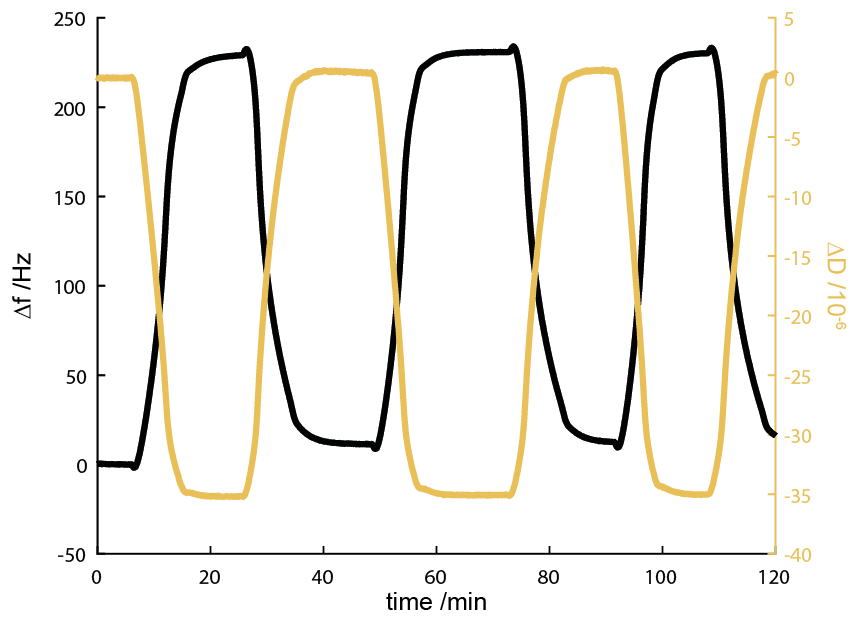
Figure A.13.: QCM-D plot of a swelling experiment for PNIPAM-co-MBAM$_1$ in PBS (pH=7.5). Three temperature increases from $22\,°C$ to $35\,°C$ reveal the reversible swell and collapse behaviour of the polymer layer.
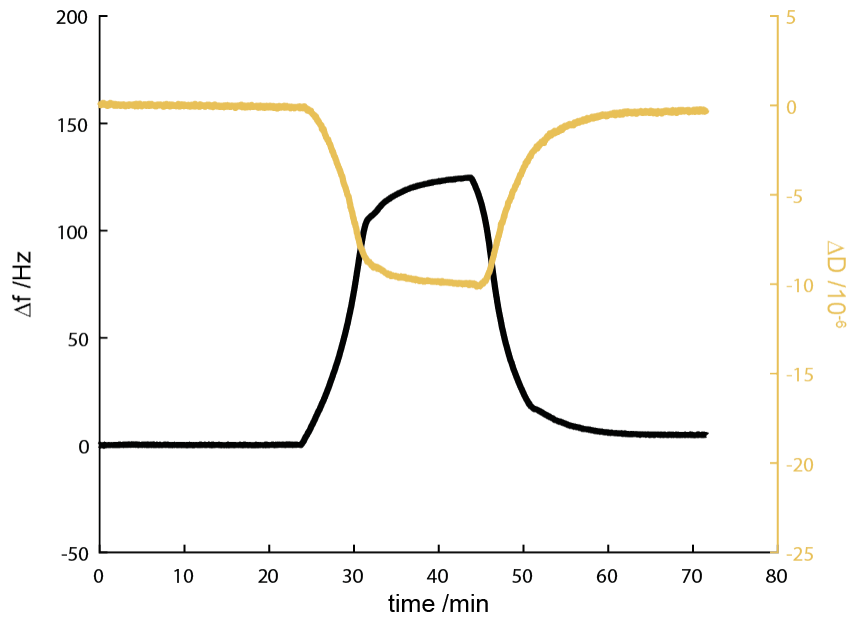
Figure A.14.: QCM-D plot of a swelling experiment for PNIPAM-co-MBAM$_3$ in PBS (pH=7.5). One temperature cycle of $22\,°C$ – $35\,°C$ – $22\,°C$ reveals the reswelling of the polymer layer back to the same extent as before the first collapse.


Figure A.15.: QCM-D plot of a swelling experiment for PNIPAM-co-MBAM$_{10}$ in PBS (pH=7.5). All three temperature increases from $22\,°C$ to $35\,°C$ show that the thermoresponsive behaviour drastically decreased within layers containing $10\,mol\%$ MBAM.
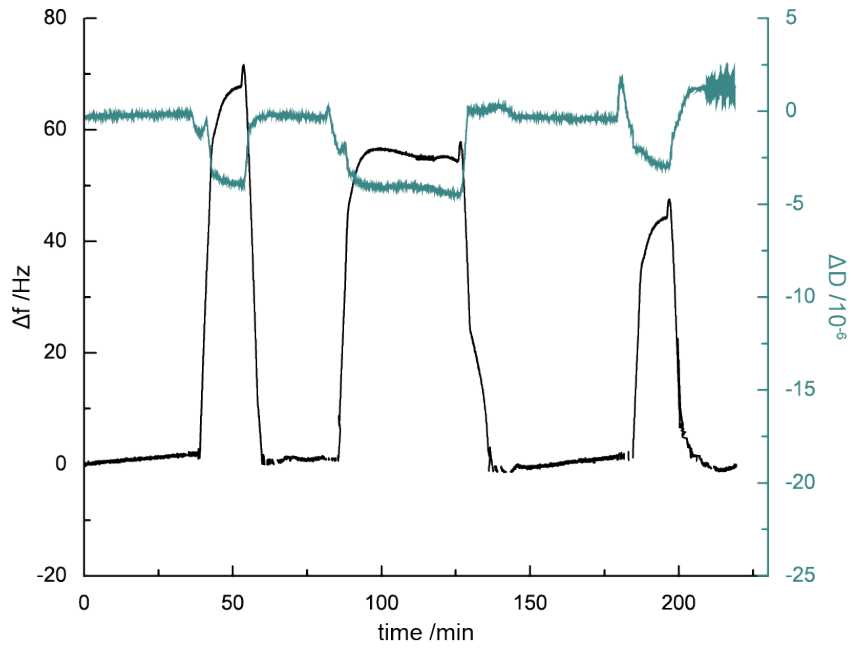
Figure A.16.: QCM-D plot of PNIPAM-co-NBPAM prepared in a mQ:dioxane=1:1 mixture in 30 min, after UV-light irradiation for 15 min.

A.3. Additional FTIR Spectra
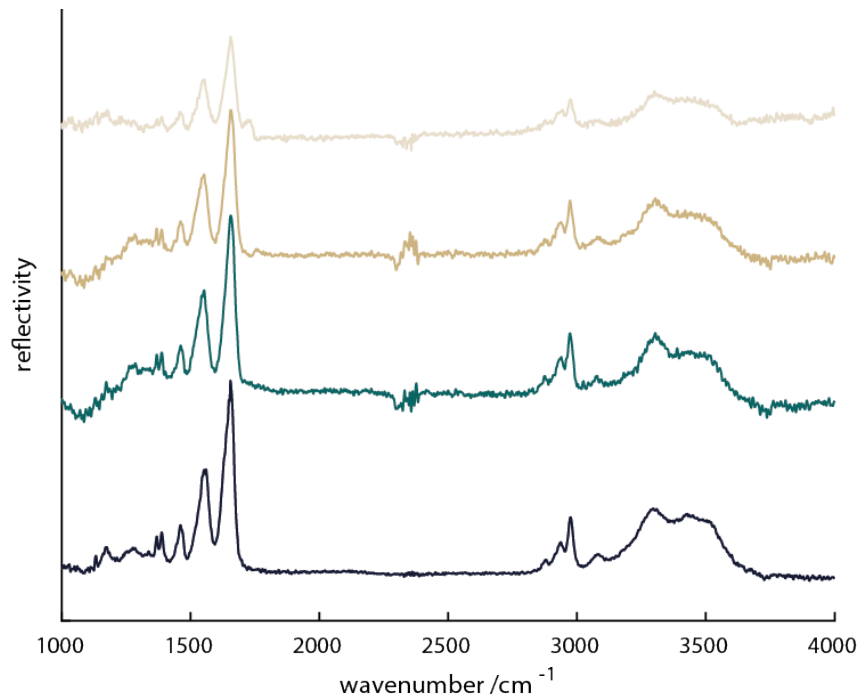
Figure A.17.: FT-IR spectra for PNIPAM-co-MBAM, containing various amounts of MBAM in this order from bottom to top: 0 mol%, 1 mol%, 2 mol%, 5 mol%.

Table A.1.: Summary of the bands observed in the FT-IR spectrum of PNIPAM. st=stretch, δ=deformation, sy=symmetric and as=asymmetric.

$\tilde{\nu}$ /cm^{-1}	involved functional groups
1250	C-N$_{st}$
1370-1390	CH$_{2\ \delta}$ & CH$_{3\ \delta,\ as}$
1450	N-H$_\delta$
1550	H-N-C=O$_{sy\ st}$
1625	hydrated -C=O
1640-1650	C=O$_{st}$ & H-bonding between C=O & H$_2$O
2870-2970	CH$_{2\ st}$ & CH$_{3\ st}$
3100-3700	N-H$_{st}$ & H$_2$O